INL/EXT-17-43056
Revision 0

Status Report on the High-Temperature Steam Electrolysis Plant Model Developed in the Modelica Framework (FY17)

Jong Suk Kim
Shannon M. Bragg-Sitton
Richard D. Boardman

August 2017

The INL is a U.S. Department of Energy National Laboratory
operated by Battelle Energy Alliance

INL/EXT-17-43056
Revision 0

Status Report on the High-Temperature Steam Electrolysis Plant Model Developed in the Modelica Framework (FY17)

Jong Suk Kim
Shannon M. Bragg-Sitton
Richard D. Boardman

August 2017

Idaho National Laboratory
Idaho Falls, Idaho 83415

http://www.inl.gov

Prepared for the
U.S. Department of Energy
Office of Nuclear Energy
Under DOE Idaho Operations Office
Contract DE-AC07-05ID14517

ABSTRACT

This report has been prepared as part of an effort to design and build a modeling and simulation (M&S) framework to assess the economic viability of a nuclear-renewable hybrid energy system (N-R HES). In order to facilitate dynamic M&S of such an integrated system, research groups in multiple national laboratories have been developing various subsystems as dynamic physics-based components using the Modelica programming language. In fiscal year 2015 (FY15), Idaho National Laboratory (INL) performed a dynamic analysis of two region-specific N-R HES configurations, including the gas-to-liquid (natural gas to Fischer-Tropsch synthetic fuel) and brackish water reverse osmosis desalination plants as industrial processes. In FY16, INL developed two additional subsystems in the Modelica framework: (1) a high-temperature steam electrolysis (HTSE) plant as a high priority industrial plant to be integrated with a light water reactor (LWR) within an N-R HES and (2) a gas turbine power plant as a secondary energy supply.

In FY17, five new components (i.e., a feedwater pump, a multi-stage compression system, a sweep-gas turbine, flow control valves, and pressure control valves) have been incorporated into the HTSE system model developed in FY16, aiming to more realistically characterize all key components of concern. Special attention has been given to the controller settings based on process models (i.e., direct synthesis method), aiming to improve process dynamics and controllability.

A dynamic performance analysis of the improved LWR/HTSE integration case was carried out to evaluate the technical feasibility (load-following capability) and safety of such a system operating under highly variable conditions requiring flexible output. The analysis (evaluated in terms of the step response) clearly shows that the FY17 model resulted in superior output responses with much smaller settling times and less oscillatory behavior in response to disturbances in the electric load than those observed with the FY16 model. Simulation results involving several case studies show that the suggested control scheme could maintain the controlled variables (including the steam utilization factor, cathode stream inlet composition, and temperatures and pressures of the process streams at various locations) within desired limits under various plant operating conditions. The results also indicate that the proposed HTSE plant could provide operational flexibility to participate in energy management at the utility scale by dynamically optimizing the use of excess plant capacity within an N-R HES.

CONTENTS

ABSTRACT v

ACRONYMS xi

1. INTRODUCTION 1

2. PROCESS MODELING AND CONTROL 1
   - 2.1 Component Description 7
     - 2.1.1 Feedwater pump (FWP) 7
     - 2.1.2 Multi-stage compression system (MSCS) 9
     - 2.1.3 Sweep-gas turbine (SGT) 10
     - 2.1.4 Flow control valves (FCVs) 11
     - 2.1.5 Pressure control valves (PCVs) 11
   - 2.2 Controller Tuning 12

3. PROCESS MODELING RESULTS 13

4. DYNAMIC PERFORMANCE ANALYSIS 15
   - 4.1 Case 1: Plant Responses during a Step Change Imposed on the VEL 16
   - 4.2 Case 2: Load-following Responses with PV Solar Power 26
   - 4.3 Case 3: Load-following Responses with Wind Power 28

5. CONCLUSIONS 30

REFERENCES 31

APPENDIX 33

FIGURES

Figure 1. Process flow diagram and control design for the LWR/HTSE integration case (FY16 model). The subscript *sp* denotes the set point. 3

Figure 2. Process flow diagram and control design for the LWR/HTSE integration case (FY17 model). 4

Figure 3. Process flow diagram and control design for the HTSE vessel (FY17 model). 5

Figure 4. Top-level model for the LWR/HTSE integration case implemented in Modelica (FY17 model). 6

Figure 5. Top-level model for the HTSE vessel implemented in Modelica (FY17 model). 7

Figure 6. Process model of the FWP with its regulatory control scheme. 8

Figure 7. Process model of the MSCS with its regulatory control scheme. 9

Figure 8. Process model of SOEC stacks with regulatory control schemes. 11

Figure 9. General energy and product flows for the LWR/HTSE integration case. The oxygen production rate is reported in parenthesis as it could possibly be recovered from the outlet anode stream by condensation if steam is used as a sweep gas instead of air. 14

Figure 10. Case 1 results following a transient at 1.67 min: (a) VEL directed to the HTSE plant ($L_{e, HTSE}$) and electrical power consumption in the SOEC stacks ($P_{e, SOEC}$), (b) electrical power consumption in the ETHs ($P_{e, ETHs}$) and in the MSCS ($P_{e, MSCS}$), and electrical power production in the SGT ($P_{e, SGT}$), (c) electrical power consumption in the FWP, (d) rate of process heat flow across the HXs, (e) hydrogen production rate, and (f) oxygen production rate. 16

Figure 11. Case 1 results – *Electrolyzer*: (a) desired (SU_{sp}) vs. actual (SU) SU factor, (b) cathode stream flow entering the HTSE vessels, (c) valve opening of the FCV that regulates the cathode stream flow entering the HTSE vessels, (d) desired ($T_{C, SOEC, out, sp}$) vs. simulated cathode stream temperature at the SOEC stack outlet ($T_{C, SOEC, out}$), (e) anode stream flow entering the HTSE vessels, and (f) valve opening of the FCV that regulates the anode stream flow entering the HTSE vessels. 18

Figure 12. Case 1 result – *Electrolyzer*: solid structure temperature gradient. 18

Figure 13. Case 1 results – *Electrolyzer*: (a) desired ($p_{C, SOEC, sp}$) vs. simulated ($p_{C, SOEC}$) SOEC stack operating pressure at the cathode side, (b) cathode stream flow exiting the HTSE vessels, (c) valve opening of the PCV that regulates the cathode stream flow exiting the HTSE vessels, (d) desired ($p_{A, SOEC, sp}$) vs. simulated ($p_{A, SOEC}$) SOEC stack operating pressure at the anode side, (e) anode stream flow exiting the HTSE vessels, and (f) valve opening of the PCV that regulates the anode stream flow exiting the HTSE vessels. 19

Figure 14. Case 1 result – *SGT*: electrical power production. 20

Figure 15. Case 1 results – *FWP*: (a) desired ($p_{C, FWP, out, sp}$) vs. simulated ($p_{C, FWP, out}$) cathode stream pressure at the FWP outlet, (b) pump shaft rotational speed, (c) power consumption, and (d) cathode stream (water) flow rate. 20

Figure 17. Case 1 results – *Nuclear-heat-recuperated HXs*: (a) desired ($T_{C, HX, out, sp}$) vs. simulated ($T_{C, HX, out}$) cathode stream temperature at the cathode HX outlet, (b) cathode stream flow rate, (c) valve opening of the TCV that regulates the steam flow entering the cathode HX, (d) desired ($T_{A, HX, out, sp}$) vs. simulated ($T_{A, HX, out}$) anode stream temperature

at the anode HX outlet, (e) anode stream flow rate, and (f) valve opening of the TCV that regulates the steam flow entering the anode HX. 22

Figure 18. Case 1 results – *ETHs*: (a) desired ($T_{C, SOEC, in, sp}$) vs. simulated ($T_{C, SOEC, in}$) cathode stream temperature at the SOEC stack inlet, (b) electric load for an ETH that heats up the cathode stream, (c) electric current for the cathode stream ETH, (d) desired ($T_{A, SOEC, in, sp}$) vs. simulated ($T_{A, SOEC, in}$) anode stream temperature at the SOEC stack inlet, (e) electric load for an ETH that heats up the anode stream, and (f) electric current for the anode stream ETH. 23

Figure 19. Case 1 results – *H_2/steam mixer*: (a) desired ($y_{C, H2, SOEC, in, sp}$) vs. simulated ($y_{C, H2, SOEC, in}$) cathode stream H_2 mole fraction at the SOEC stack inlet, (b) steam flow rate, and (c) recycled hydrogen flow rate. 24

Figure 20. Model comparisons (FY16 vs. FY17): (a) VEL directed to the HTSE plant ($L_{e, HTSE}$), (b) SU factor (*SU*), (c) cathode stream temperature at the SOEC stack outlet ($T_{C, SOEC, out}$), (d) cathode stream H_2 mole fraction at the SOEC stack inlet ($y_{C, H2, SOEC, in}$), (e) cathode stream temperature at the cathode HX outlet ($T_{C, HX, out}$), (f) anode stream temperature at the anode HX outlet ($T_{A, HX, out}$), (g) cathode stream temperature at the SOEC stack inlet ($T_{C, SOEC, in}$), and (h) anode stream temperature at the SOEC stack inlet ($T_{A, SOEC, in}$). 25

Figure 21. Case 2 results: (a) PV solar power generation, and (b) hydrogen (w_{H2}) and oxygen (w_{O2}) production rates. 26

Figure 22. Case 2 results: (a) SU factor, (b) cathode stream H_2 mole fraction at the SOEC stack inlet, (c) SOEC stack operating pressure at the anode side, (d) cathode stream pressure at the FWP outlet, (e) cathode stream temperature at the cathode HX outlet, (f) anode stream temperature at the anode HX outlet, (g) cathode stream temperature at the SOEC stack inlet, and (h) cathode stream temperature at the SOEC stack outlet. 27

Figure 23. Case 3 results: (a) wind power generation, and (b) hydrogen (w_{H2}) and oxygen (w_{O2}) production rates. 28

Figure 24. Case 3 results: (a) SU factor, (b) cathode stream H_2 mole fraction at the SOEC stack inlet, (c) SOEC stack operating pressure at the anode side, (d) cathode stream pressure at the FWP outlet, (e) cathode stream temperature at the cathode HX outlet, (f) anode stream temperature at the anode HX outlet, (g) cathode stream temperature at the SOEC stack inlet, and (h) cathode stream temperature at the SOEC stack outlet. 29

TABLES

Table 1. Model input parameters and process variables for the FWP at the nominal operating condition. 8

Table 2. Model input parameters and process variables for the MSCS at the nominal operating condition. 10

Table 3. Model input parameters and process variables for the SGT at the nominal operating condition. 10

Table 4. Regulatory controllers used in the HTSE plant. 12

Table 5. Hydrogen production summary. 14

Table 6. Simulation setup values used in the case studies for the LWR/HTSE integration. 15

Table A. PI controller settings based on the DS method. 33

ACRONYMS

CTRL	Controller
CV	Controlled variable
DS	Direct synthesis
Dymola	Dynamic modeling library
ETH	Electric topping heater
FCV	Flow control valve
FOPTD	First-order-plus-time-delay
FWP	Feedwater pump
FY	Fiscal year
HTSE	High-temperature steam electrolysis
HX	Heat exchanger
IC	Intermediate cooler
IGV	Inlet guide vanes
INL	Idaho National Laboratory
ISO	International organization for standardization
LWR	Light water reactor
M&S	Modeling and simulation
MSCS	Multi-stage compression system
MV	Manipulated variable
N-R HES	Nuclear-renewable hybrid energy system
PCV	Pressure control valve
PI	Proportional-integral
PR	Pressure ratio
PV	Photovoltaic
SGT	Sweep-gas turbine
SOEC	Solid oxide electrolysis cell
SOFC	Solid oxide fuel cell
SOPTD	Second-order-plus-time-delay
SU	Steam utilization
TCV	Temperature control valve
VEL	Variable electrical load

Status Report on the High-Temperature Steam Electrolysis Plant Model Developed in the Modelica Framework (FY17)

1. INTRODUCTION

This report provides the current status on component models developed in the *Modelica*[1] framework at Idaho National Laboratory (INL) under the nuclear-renewable hybrid energy system (N-R HES) program. In fiscal year 2015 (FY15), INL identified two region-specific N-R HES configurations to be located in West Texas and Arizona for preliminary technical and operational economic analysis [1-6]. The first configuration employs a nuclear plant and a series of wind turbines to produce electricity and convert carbon resources (natural gas) to synthetic liquid fuels (gasoline and diesel) using excess thermal capacity. The second configuration employs a nuclear plant and solar photovoltaic (PV) stations for energy generation, and yields electricity to meet grid demand and to produce fresh water via reverse osmosis desalination using excess electrical capacity. Both systems have been implemented in the Modelica framework [7]. In FY16, INL developed two additional subsystem models: a high-temperature steam electrolysis (HTSE) plant, which employs planar solid oxide electrolysis cells (SOECs), and a gas turbine power plant [8].

In FY17, the HTSE plant model developed in FY16 was modified and improved to include several key components of the plant that had not been taken into account previously. In addition, the proportional-integral (PI) controller parameters were tuned to improve the dynamic responses of the considered HTSE configuration. To demonstrate the effectiveness of the process design, and control and instrumentation strategies proposed for the improved HTSE system, numerous tests were carried out under highly flexible operations. In particular, the technical performance of the considered system was evaluated in terms of step and load-following responses. In order to assess the load-following capability of the improved HTSE plant, two types of renewable energy sources (i.e., PV and wind energy) were considered. They were used to replicate the situation in which excess electrical power directed to the HTSE process is identical to variable renewable generation, with a constant load imposed by the electric grid. As the emphasis is on a detailed investigation of dynamic performance characteristics of the proposed HTSE system under variable operating conditions, mathematical modeling details (i.e., specific governing equations derived from first principles) are not provided in this report.

The reminder of this report is organized into four sections. Section 2 presents an overview of the process modeling and control of the improved HTSE system. The results of the process modeling are discussed in Section 3. Section 4 provides dynamic simulation results involving several case studies with detailed discussion. Finally, Section 5 concludes this report.

2. PROCESS MODELING AND CONTROL

This section is dedicated to process modeling and control of several new components added to the HTSE configuration proposed in FY16. Figure 2, as a comparison, shows the process details of the HTSE configuration proposed in FY16 to simulate integration of a light water reactor (LWR) with the HTSE process, and the associated regulatory control design [8]. As seen in this figure, ten main components can be identified as follows:

[1] *Modelica* is an object-oriented, equation-based programming language suitable for computational applications with high complexity requiring high performance.

Physical devices
1. SOEC stacks
2. Heat exchangers (HXs) (or heat recuperators)
3. Electric topping heaters (ETHs)
4. Hydrogen/steam mixer
5. Hydrogen recycle loop
6. Flash drum
7. Switchyard

Control devices

8. Classical feedback controllers (CTRLs)
9. Feedforward controllers
10. Temperature control valves (TCVs)

For detailed component description, see FY16 report [8].

In FY17, five new components have been incorporated into the HTSE system developed in FY16 to more realistically characterize all key components of concern as follows:

Physical devices
1. Feedwater pump (FWP)
2. Multi-stage compression system (MSCS)
3. Sweep-gas turbine (SGT)

Control devices

4. Flow control valves (FCVs)
5. Pressure control valves (PCVs)

Process details of the LWR/HTSE integration case, including new components, and associated regulatory control design are shown in Figures 2 and 3.

In this report, the Modelica models were implemented using the commercially available Modelica-based modeling and simulation (M&S) environment, i.e., a dynamic modeling library (Dymola) version 2017 FD01 [9]. In-house developed packages and open-source libraries were utilized to facilitate M&S. In particular, the *Modelica standard library* version 3.2.2 [10] and *ThermoPower library* version 3.1beta.0 [11] were utilized. M&S were conducted in compliance with the Modelica code standards [8, 12, 13]. The plant model was developed on a Dell Precision M4800 with Intel® Core™ i7-4940MX CPU (quad core extreme 3.10 GHz) and with 32.0 GB of RAM (1600 MHz DDR3L). Figures 4 and 5 show the Modelica models (which correspond to Figures 2 and 3, respectively) implemented within the Dymola development environment.

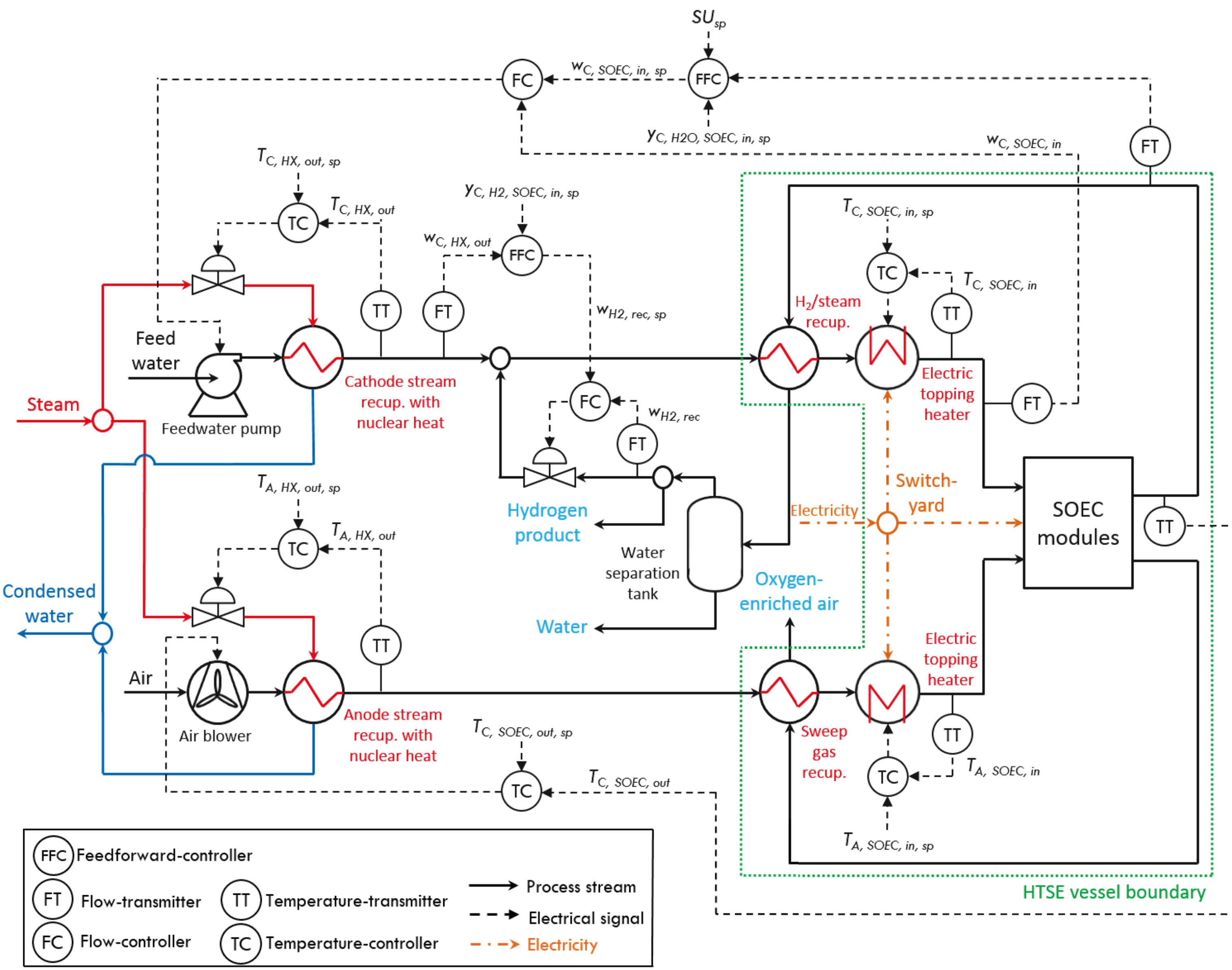

Figure 1. Process flow diagram and control design for the LWR/HTSE integration case (FY16 model). The subscript *sp* denotes the set point.

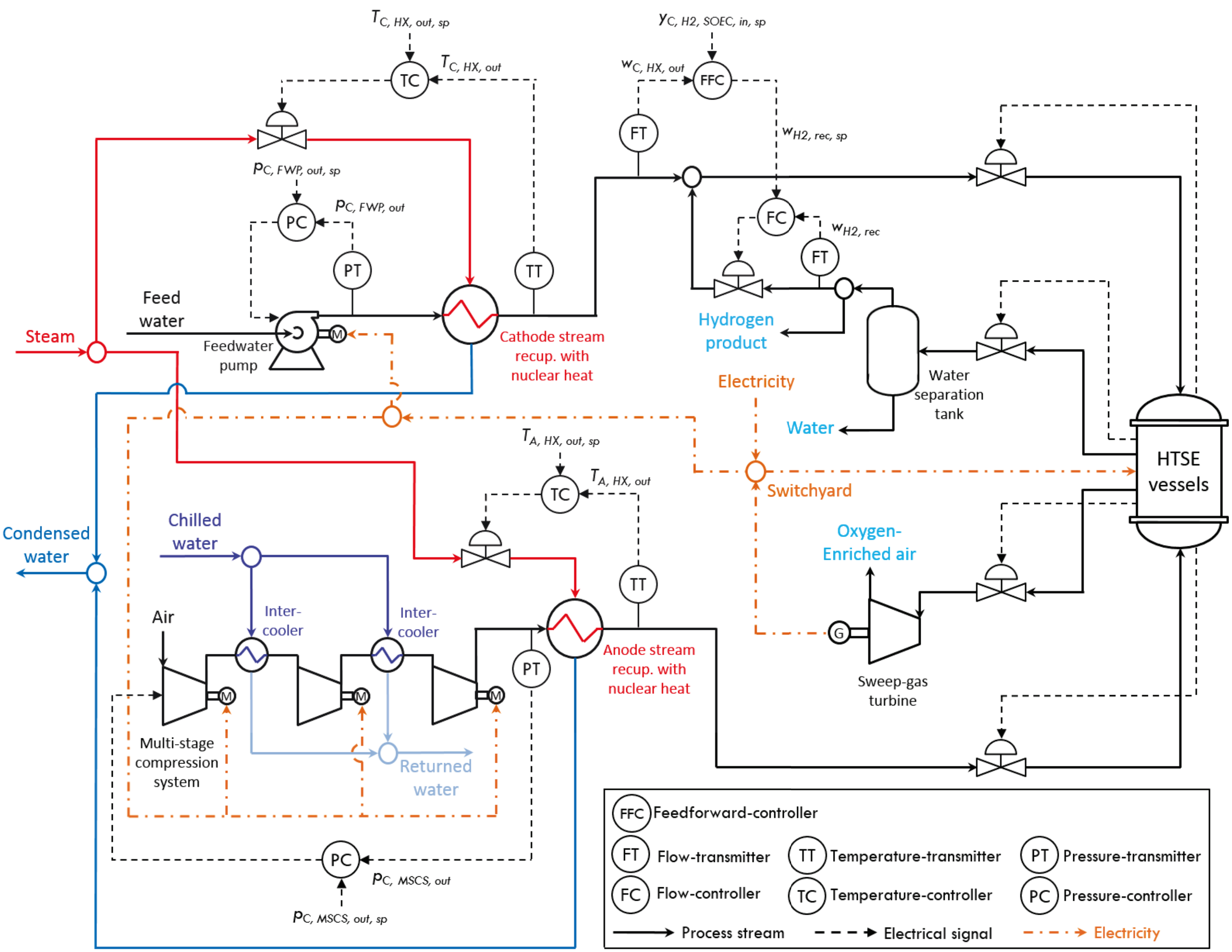

Figure 2. Process flow diagram and control design for the LWR/HTSE integration case (FY17 model).

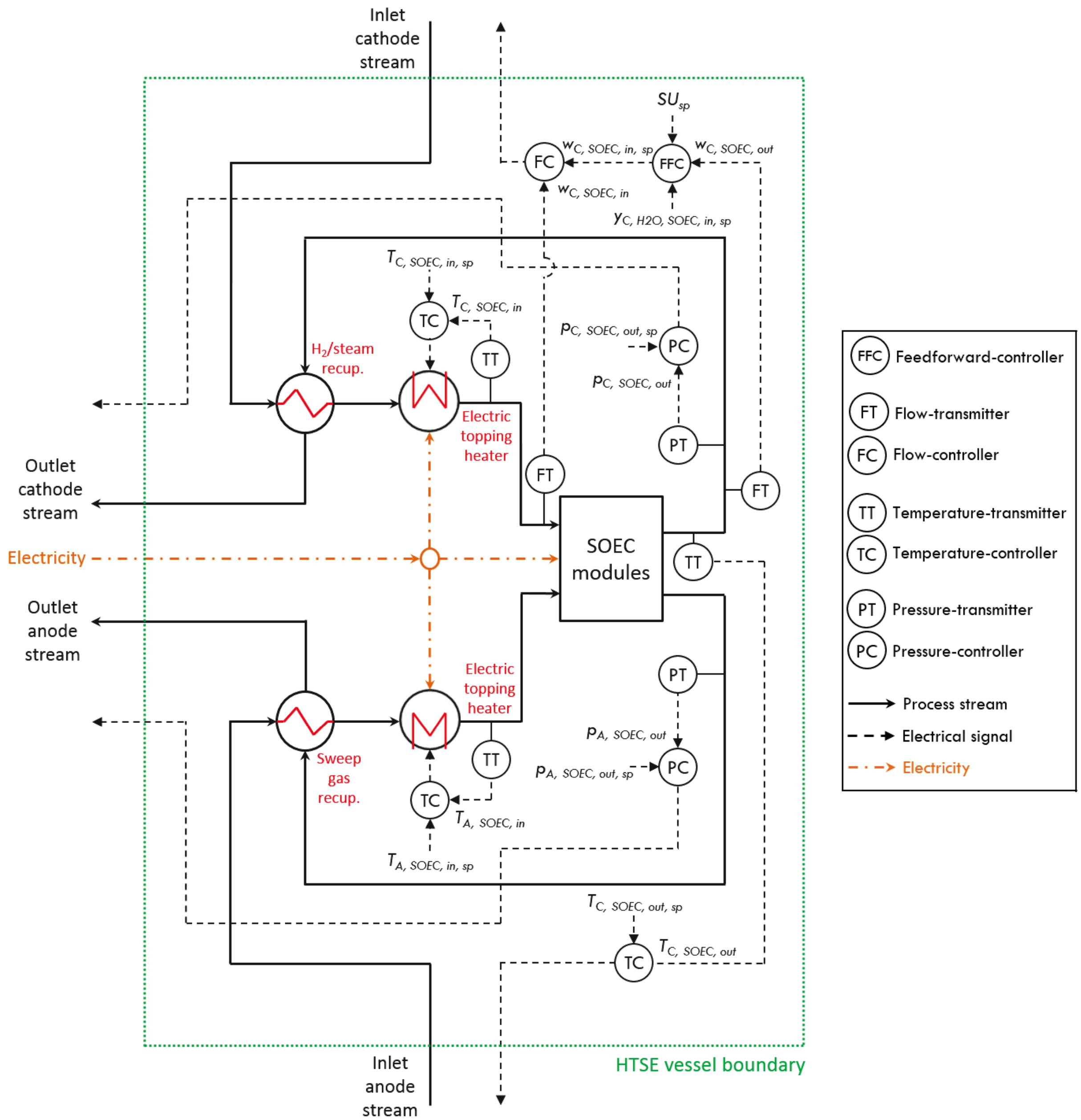

Figure 3. Process flow diagram and control design for the HTSE vessel (FY17 model).

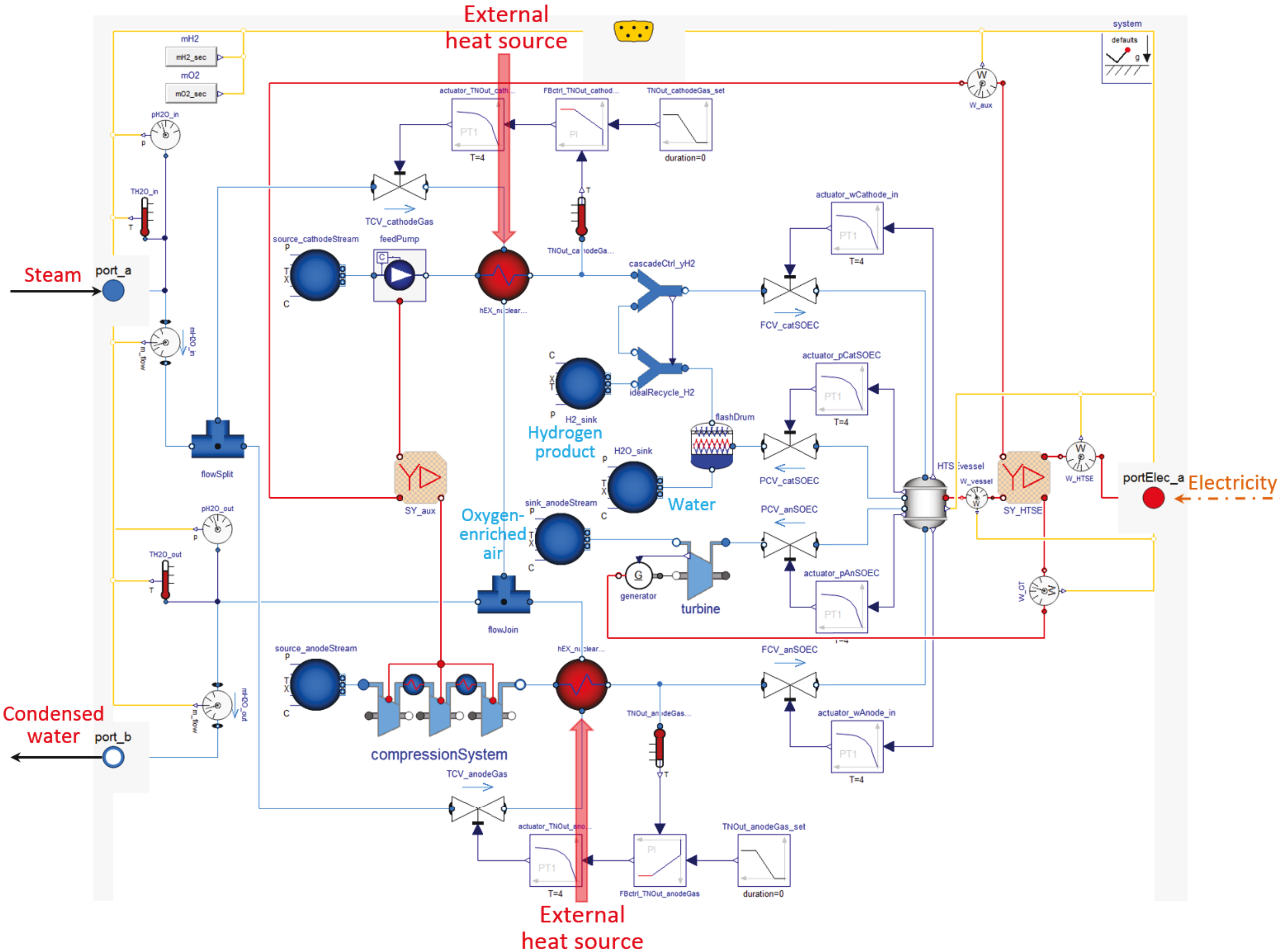

Figure 4. Top-level model for the LWR/HTSE integration case implemented in Modelica (FY17 model).

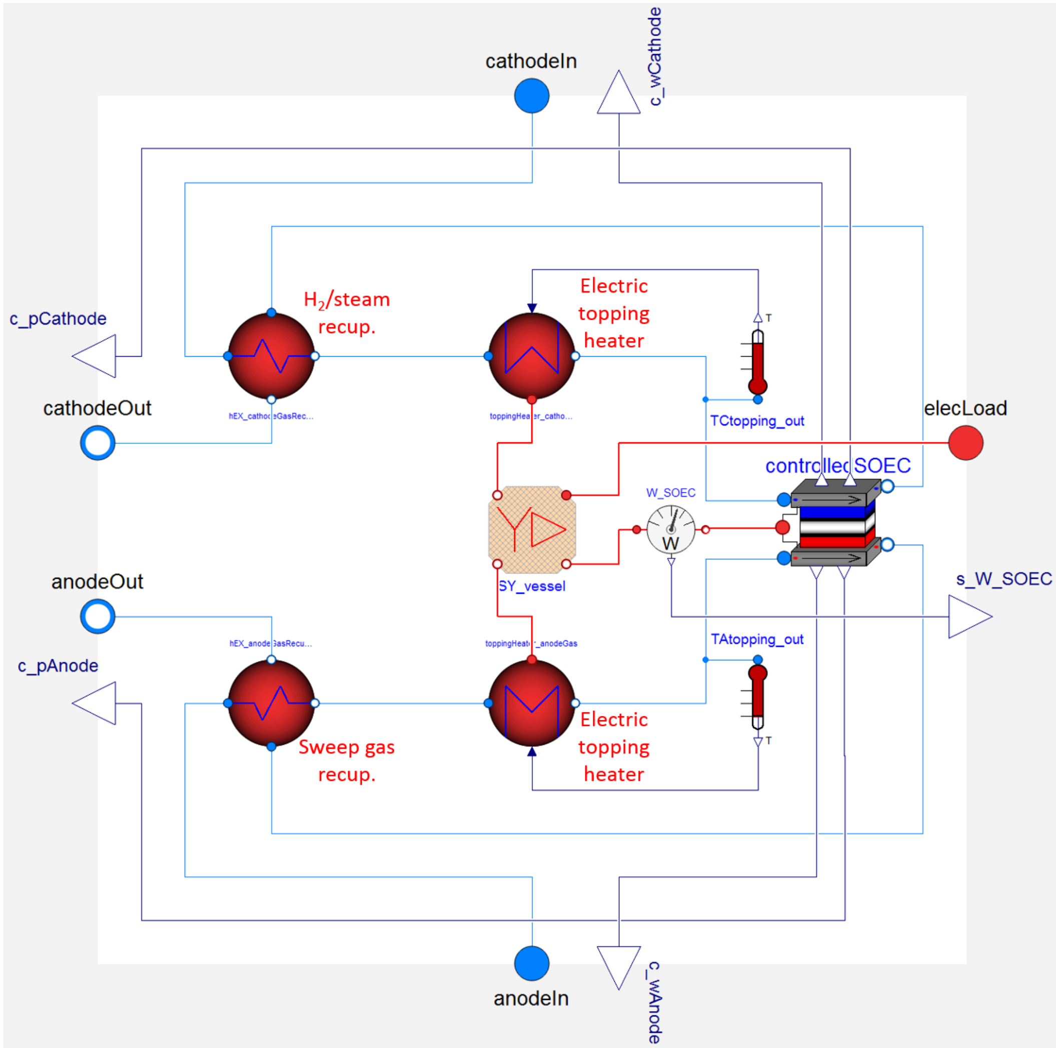

Figure 5. Top-level model for the HTSE vessel implemented in Modelica (FY17 model).

2.1 Component Description

This section provides a description of each of the new components, which consist of a number of basic subcomponents that are also introduced. Detailed descriptions of the basic subcomponents are beyond the scope of this report.

2.1.1 Feedwater pump (FWP)

In FY16, the cathode feed stream (liquid water) was assumed to be pre-compressed at a desired pressure level; thus, the HTSE vessels, which contain the SOEC stacks and ETHs, are the only units that consume the electricity in the HTSE plant. In FY17, liquid water feedstock at a pressure of 1 atm (0.101325 MPa) and a temperature of 25°C is assumed to enter a centrifugal FWP, which compresses the feed to 2.37 MPa (a set point for the FWP outlet pressure, $p_{C,\,FWP,\,out,\,sp}$). Several advantages are expected if the HTSE process is operated at elevated pressure:

- Elevated pressure supports higher mass flow rates for the same size components, facilitating downstream production of hydrogen (H_2).

- Less energy consumption is required for pressurizing steam by evaporating liquid water as compared to pressurizing the gaseous hydrogen product, which will ultimately be delivered at elevated pressure either for storage or pipeline.
- The performance of (cathode-supported) SOECs can be improved by pressurization, as increasing pressure would result in an increase in gas diffusion rates and therefore a decrease in the concentration overpotential [14].

This compressed liquid water then enters the nuclear-heat-recuperated cathode HX where the stream is vaporized and superheated (see Figure 2). Table 1 summarizes the design specifications of the FWP.

Table 1. Model input parameters and process variables for the FWP at the nominal operating condition.

Description	Unit	Value
Power consumption	MW_e	0.0127
Flow rate	kg s^{-1}	4.485
Pump shaft rotational speed	rpm	1500
Fluid density	kg m^{-3}	998
Outlet temperature	°C	25.2
Outlet pressure	MPa	2.37
Pump efficiency	%	80

Figure 6 presents the FWP model, along with its control strategy, implemented in Modelica. The cathode stream pressure at the FWP outlet ($p_{C,\ FWP,\ out}$) is controlled by adjusting the pump shaft rotational speed through a PI controller.

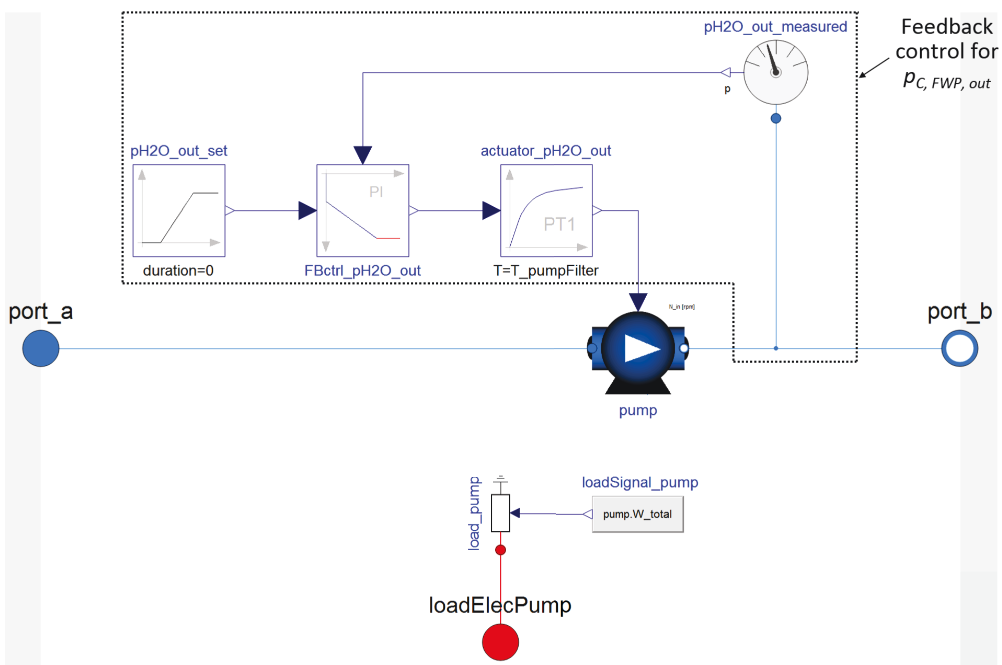

Figure 6. Process model of the FWP with its regulatory control scheme.

2.1.2 Multi-stage compression system (MSCS)

In FY16, the anode feed stream (air) was assumed to be pre-compressed at a desired pressure level prior to entering the anode HX. In FY17, air feedstock at typical international organization for standardization (ISO) conditions (i.e., 0.101325 MPa and 15°C [15]) is assumed to enter an MSCS (a three-stage compressor with intercooling), which compresses the feed to 2.37 MPa (a set point for the MSCS outlet pressure, $p_{A,\ MSCS,\ out,\ sp}$). Compared to single-stage compression, multi-stage compression is advantageous in several ways:

- The work done in compressing air is reduced, thus power can be saved.
- Volumetric efficiency of a compressor increases due to reduced pressure ratio (PR) in each stage.
- Wall thickness of the compressor housing is reduced since it has to withstand lower pressures, resulting in a lighter and cheaper compressor.

Figure 7 presents the MSCS model, along with its control strategy, implemented in Modelica. Initially, the intake of air in the first stage gets compressed and heated. The heated air then passes over an intermediate cooler (IC) where the stream is cooled to about 40°C using the chilled water. This cooled air enters the second stage where it is again compressed and heated. Finally, after being cooled to 40°C in an IC, the air is passed to the final stage of the MSCS where it is compressed to the required pressure. The final compression stage is not followed by a cooler as air needs to be heated afterwards [16]. Therefore, the air exiting the MSCS enters the anode HX at about 189°C where its temperature is further amplified using nuclear process heat (see Figure 2). As described in Figure 7, the anode stream pressure at the MSCS outlet ($p_{A,\ MSCS,\ out}$) is controlled by adjusting the compressor inlet guide vane (IGV) angle through an "integral-only" controller.

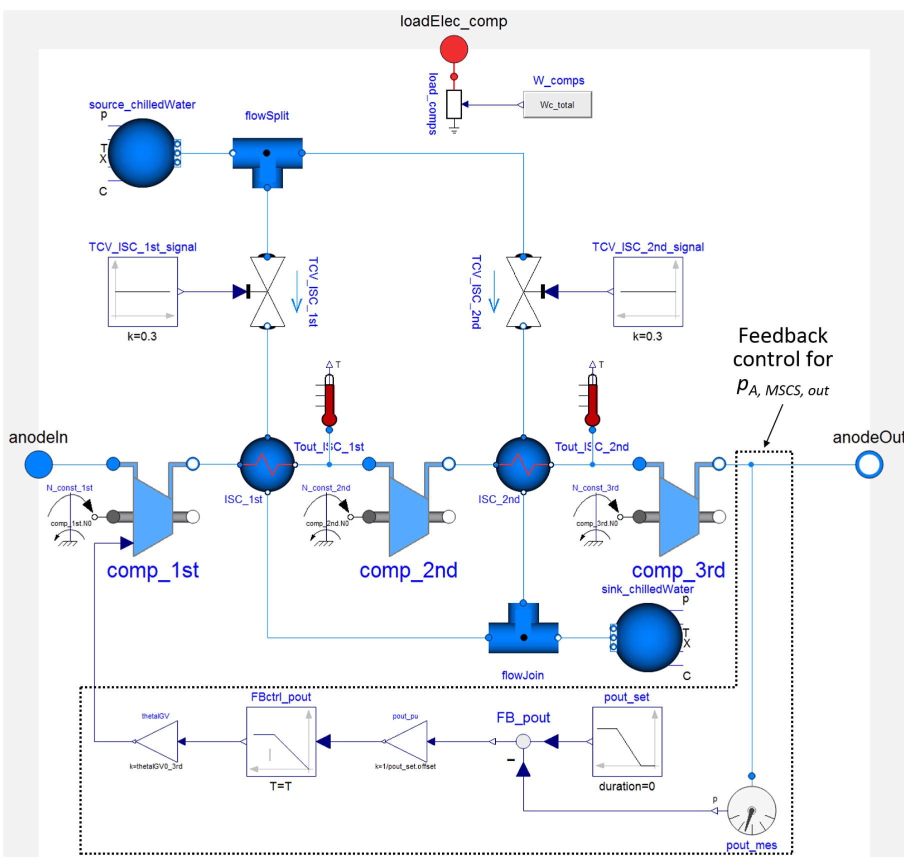

Figure 7. Process model of the MSCS with its regulatory control scheme.

Table 2 reports the design specifications of the MSCS.

Table 2. Model input parameters and process variables for the MSCS at the nominal operating condition.

Description	Unit	Value
Power consumption	MW_e	10.1
Flow rate	$kg\ s^{-1}$	23.3
IGV angle	degree	50.1
Chilled water inlet temperature	°C	7
Outlet temperature at the 1^{st} stage	°C	140
Outlet temperature at the 2^{nd} stage	°C	182
Outlet temperature at the 3^{rd} stage	°C	189
PR at each stage	–	3.046
Outlet pressure at the 1^{st} stage	MPa	0.3086
Outlet pressure at the 2^{nd} stage	MPa	0.8182
Outlet pressure at the 3^{rd} stage	MPa	2.37
Isentropic efficiency of the 1^{st} stage	%	86
Isentropic efficiency of the 2^{nd} stage	%	82
Isentropic efficiency of the 3^{rd} stage	%	78
Mechanical efficiency	%	98

2.1.3 Sweep-gas turbine (SGT)

In FY16, the anode stream (sweep gas) exiting the electrolyzer at a fairly high pressure (1.923 MPa) was released to open air without further energy recovery. In FY17, some of the sweep gas compression work (around 78.6%) is recovered using an SGT located at the sweep-gas exit (see Figure 2). Table 3 summarizes the design specifications of the SGT.

Table 3. Model input parameters and process variables for the SGT at the nominal operating condition.

Description	Unit	Value
Power generation	MW_e	7.89
Flow rate	$kg\ s^{-1}$	26.5
Turbine shaft rotational speed	rpm	3600
Inlet temperature	°C	333
Outlet temperature	°C	35.1
Inlet pressure	MPa	1.73
Outlet pressure	MPa	0.101325
Turbine efficiency	%	89
Mechanical efficiency	%	98

2.1.4 Flow control valves (FCVs)

In FY16, output signals from the controllers that regulate the *steam utilization* (*SU*) *factor*[2] and SOEC stack temperature were directly input to the *ideal flow sources*,[3] which produced the requested cathode and anode mass flow rates (see Figure 1). In order words, the controllers' output signals were manipulated to set the mass flow rates, without employing actuators. In FY17 the two pneumatic FCVs were incorporated into the HTSE system in order to manipulate the cathode and anode mass flow rates, which regulate the SU factor and SOEC stack temperature, respectively (see Figure 2).

2.1.5 Pressure control valves (PCVs)

In FY17, two PCVs were introduced to maintain the desired electrolysis operating pressure (1.964 MPa) at both the cathode ($p_{C,\ SOEC}$) and anode ($p_{A,\ SOEC}$) sides of the SOEC stack (Figure 8). The stack pressure on the cathode side is controlled by the PCV located between the flash drum (water knockout tank) and the HTSE vessels, whereas the stack pressure on the anode side is controlled by the PCV located between the SGT and the HTSE vessels.

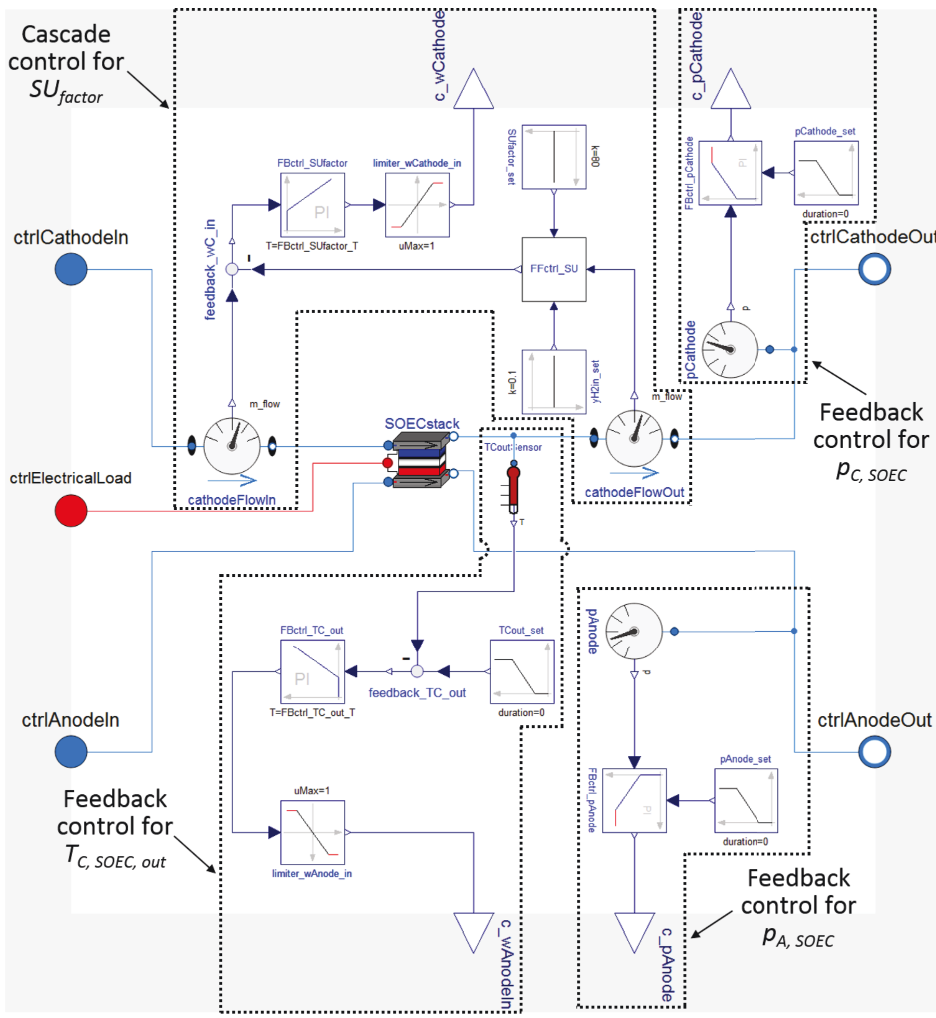

Figure 8. Process model of SOEC stacks with regulatory control schemes.

---

[2] The *steam utilization factor* is the percentage of the total inlet stream flow that is consumed by the electrolysis reaction [8].

[3] An *Ideal flow source* is a Modelica subcomponent model that produces a prescribed mass flow with prescribed temperature and mass fraction [10].

2.2 Controller Tuning

Numerous feedback/feedforward controllers were augmented as low-level (regulatory) controllers to maintain the desired process conditions, such as temperatures, pressures, mass flow rates, and mole fractions at various locations in the considered HTSE plant. For the classical feedback control scheme implemented in this report, control actions (values) were calculated by PI controllers in all cases, except the one implemented for the anode stream pressure control. Table 4 summarizes the controllers (single-input single-output scheme), with their set-point values, used in the proposed HTSE system.

Table 4. Regulatory controllers used in the HTSE plant.

CTRL No.	Functionality	Controller type	Controlled variable	Set-point value
1	Regulate cathode stream temperature	Feedback (PI)	Cathode stream temperature at the cathode HX outlet	283.4°C
2	Regulate anode stream temperature	Feedback (PI)	Anode stream temperature at the anode HX outlet	259°C
3	Regulate cathode stream composition	Cascade (feedforward/ feedback [PI])	Cathode stream H_2 mole fraction at the SOEC stack inlet	0.1
4	Regulate cathode stream temperature	Feedback (PI)	Cathode stream temperature at the SOEC stack inlet	850°C
5	Regulate anode stream temperature	Feedback (PI)	Anode stream temperature at the SOEC stack inlet	850°C
6	Regulate SOEC stack temperature	Feedback (PI)	Cathode stream temperature at the SOEC stack outlet	750°C
7	Regulate steam consumption during electrolysis	Cascade (feedforward/ feedback [PI])	SU factor	80%
8	Regulate cathode stream pressure	Feedback (PI)	Cathode stream pressure at the FWP outlet	2.37 MPa
9	Regulate anode stream pressure	Feedback (integral-only)	Anode stream pressure at the MSCS outlet	2.37 MPa
10	Regulate cathode stream pressure	Feedback (PI)	SOEC stack pressure at the cathode side	1.964 MPa
11	Regulate anode stream pressure	Feedback (PI)	SOEC stack pressure at the anode side	1.964 MPa

Notes: CTRLs 8–11 were added in FY17. CTRL 9 is an “integral-only” controller.

In FY16, although the controlled variables (CVs) listed in Table 4 (CTRL No. 1–7) could be maintained adequately close to their set-point values under various plant operating conditions, *control tuning*[4] was not properly performed. If a reasonably accurate dynamic model of the process is available, it is advantageous to base the controller design on the process model [17]. In this regard, controller settings for the considered HTSE plant were determined based on process models in the FY17 work in order to improve process dynamics and controllability.

Among the various techniques available to determine controller feedback settings, such as the direct synthesis (DS) method, internal model control method, controller tuning relations and frequency response techniques, the DS method was employed to tune the PI controller settings with the assumptions that the process models are approximated by either the first-order-plus-time-delay (FOPTD) or second-order-plus-time-delay (SOPTD) model. In either case, the model was assumed to be perfect (no model error). The results are summarized in Table A in the Appendix. For detailed reading on the DS method, see Ref. [17]. The effectiveness of the suggested controller settings is fully examined with case studies in Section 4.1.

3. PROCESS MODELING RESULTS

Figure 9 graphically presents a high-level material and energy balance summary for the LWR/HTSE integration case at the nominal operating condition. A summary of the modeling results is provided in Table 5. The HTSE plant uses a total of 61.2 MW_e electrical power, of which 45.5 MW_e (74.3%) is consumed by the electrolysis reaction within the SOEC stacks. The electric power used in the FWP is negligible compared to the total power consumption in the HTSE plant. By recovering some of the sweep gas compression work 7.89 MW_e (via the SGT), the electrical load input from the nuclear reactor to the HTSE process is reduced to 53.3 MW_e (12.9%). A thermal energy of 14.6 MW_{th} [4.63 MW_e] from the nuclear reactor is used to convert the feed water to low-temperature steam and to heat the sweep gas (air), which amounts to about 8% of the total energy consumption in the HTSE plant. Overall, the combined electrical power and heat directed to the HTSE plant from an N-R HES is about 182 MW_{th} (or 57.9 MW_e), applying a fixed thermal-to-electrical conversion efficiency of 31.8%.

The nominal value of the cathode stream flow (4.48 kg s^{-1}) is selected to achieve the SU factor of 80%, given that a cathode stream H_2 mole fraction at the SOEC stack inlet is 0.1. The nominal value of the anode stream flow rate (23.3 kg s^{-1}) is selected to achieve the cathode stream outlet temperature of 750°C, creating the temperature difference of 100°C between the inlet and outlet in the SOEC stack. The temperature gradient of this scale is expected to result in significant convective heat transfer between the cell components and air flow. At nominal operating conditions this system can produce 0.4015 kg s^{-1} (12.7 metric ton yr^{-1}) hydrogen without generating carbon dioxide (CO_2). If steam is used as a sweep gas instead of air supplied to the anode side of the SOEC, the “assumed” oxygen production rate corresponds to 3.186 kg s^{-1} (100 metric ton yr^{-1}).

[4] *Control tuning* is a procedure to achieve the desired closed-loop system performance by adjusting the controller settings.

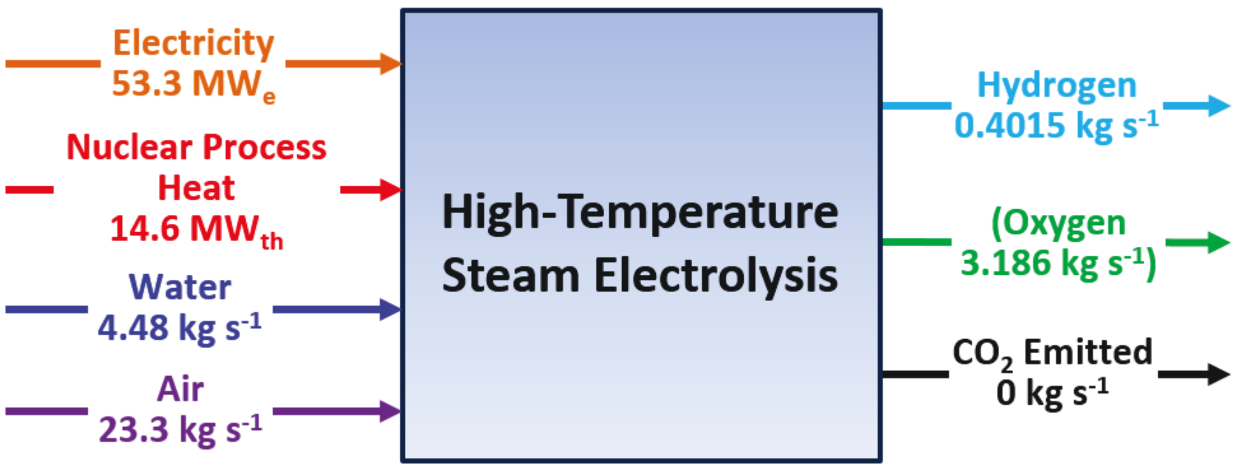

Figure 9. General energy and product flows for the LWR/HTSE integration case. The oxygen production rate is reported in parenthesis as it could possibly be recovered from the outlet anode stream by condensation if steam is used as a sweep gas instead of air.

Table 5. Hydrogen production summary.

	Description		Unit	Value
Inputs	Water		kg s^{-1} [metric ton yr^{-1}]	4.48 [141]
	Air		kg s^{-1} [metric ton yr^{-1}]	23.3 [734]
Outputs	Hydrogen		kg s^{-1} [metric ton yr^{-1}]	0.4015 [12.7]
	(Oxygen)		kg s^{-1} [metric ton yr^{-1}]	3.186 [100]
	CO_2		kg s^{-1} [metric ton yr^{-1}]	0 [0]
Utility summary	Power consumption	Total	MW_e [MW_{th}]	61.2 [192.5[a]]
		Electrolyzer	MW_e [MW_{th}]	45.5 [143.2[a]]
		MSCS	MW_e [MW_{th}]	10.1 [31.6[a]]
		FWP	MW_e [MW_{th}]	0.0127 [0.0401[a]]
		ETHs	MW_e [MW_{th}]	5.61 [17.7[a]]
	Power generation	SGT	MW_e [MW_{th}]	7.89 [24.8[a]]
	Nuclear process heat		MW_{th} [MW_e]	14.6 [4.63[b]]

[a] The thermal equivalent of the electrical power with thermal efficiency of 31.8%.
[b] The rate of heat flow expressed in terms of the electrical power equivalent with thermal efficiency of 31.8%.

4. DYNAMIC PERFORMANCE ANALYSIS

Three case studies (Cases 1–3) are conducted to analyze the dynamic performance of the LWR/HTSE integration case proposed in FY17. The key process variables (CVs listed in Table 4 and their corresponding manipulated variables [MVs], as well as hydrogen and oxygen production rates) are observed to evaluate the technical feasibility and safety of such a system operating under highly flexible conditions. Key assumptions employed for the case studies are as follows:

- A power-smoothing battery is used to smooth the high variability introduced by either PV or wind energy, acting as a low-pass filter. The power-smoothing effect of such an electric battery is modeled as a first-order differential equation with a time constant of 1800 s (30 min) [8].
- Renewable energy generation is modeled as a time-series input signal to the power-smoothing battery based on solar irradiance and ambient temperature data for a PV system or based on wind speed data for a wind farm [8, 18]. Historical data for solar irradiance and ambient temperature at Southwest Solar Research Park in Phoenix, Arizona[5] and that of wind speed measured in West Texas[6] were obtained from the National Renewable Energy Laboratory database for use in the case studies. For the mathematical models and the values of model parameters used to calculate PV solar and wind powers in this report, see Refs. [4, 5].
- At typical SOEC stack temperatures and irreversible losses values, operation at the thermoneutral voltage yields current densities in the 0.2–0.6 A cm^{-2} range, which is very close to the current density range that has yielded successful long-term operation in solid oxide fuel cell stacks [19]. For this reason, the minimum turndown of the HTSE plant (24 MW_e, of which 16.6 MW_e is delivered to the SOEC stacks) is selected to correspond to the lower bound of the considered current density range. This ensures that the plant is operated continuously with a minimum load, even when no renewable power is provided to the system. Thus, within N-R HESs, it is assumed that a minimum load of 24 MW_e is always distributed to the HTSE process.

Table 6 lists the simulation setup values used in each case scenario considered.

Table 6. Simulation setup values used in the case studies for the LWR/HTSE integration.

Case No.	Renewable energy		Electrical load delivered to HTSE process, $L_{E,\,HTSE}$ (MW_e)	Simulation output interval, Δt (s)
	Type	Generation (MW_e)		
1	N/A	0	53.3 to 45.3 (step change)	1
2	PV solar	0–30	24–54 (variable)	60
3	Wind	0–28.8	24–52.8 (variable)	60

[5] Accessed on August 7, 2017 at http://www.nrel.gov/midc/ssrp/

[6] Accessed on August 8, 2017 at http://www.nrel.gov/grid/wind-integration-data.html

4.1 Case 1: Plant Responses during a Step Change Imposed on the VEL

A step change in the variable electrical load (VEL) directed to the HTSE plant ($L_{e,\,HTSE}$) has been imposed, replicating the situation in which changes in the supply of input electrical power are experienced (e.g. from a renewable supply or the sudden switch-off of the stack). Initially, the system has settled to its nominal operating condition. The transient was initiated at 1.67 min (100 s) via an 8 MW_e step decrease in the $L_{e,\,HTSE}$ from an initial load level of 53.3 MW_e (Figure 10(a)). The VEL input was subsequently apportioned (via the switchyard) among the various system components, i.e. the electrolyzer ($P_{e,\,SOEC}$ in Figure 10(a)), the ETHs ($P_{e,\,ETHs}$ in Figure 10(b)), the MSCS ($P_{e,\,MSCS}$ in Figure 10(b)), and the FWP (Figure 10(c)). It can be seen from Figure 10(d) that as the $L_{e,\,HTSE}$ decreased, so did the thermal energy consumed for heat recuperation in the HXs; however, decreased $L_{e,\,HTSE}$ resulted in an increased SGT power output ($P_{e,\,SGT}$ in Figure 10(b)). Detailed discussion for this behavior is provided with figures later in this section. As can be seen, both the hydrogen (Figure 10(e)) and oxygen (Figure 10(f)) production rates are proportional to the load, i.e., an average current density is directly proportional to the electrolysis reaction rate.

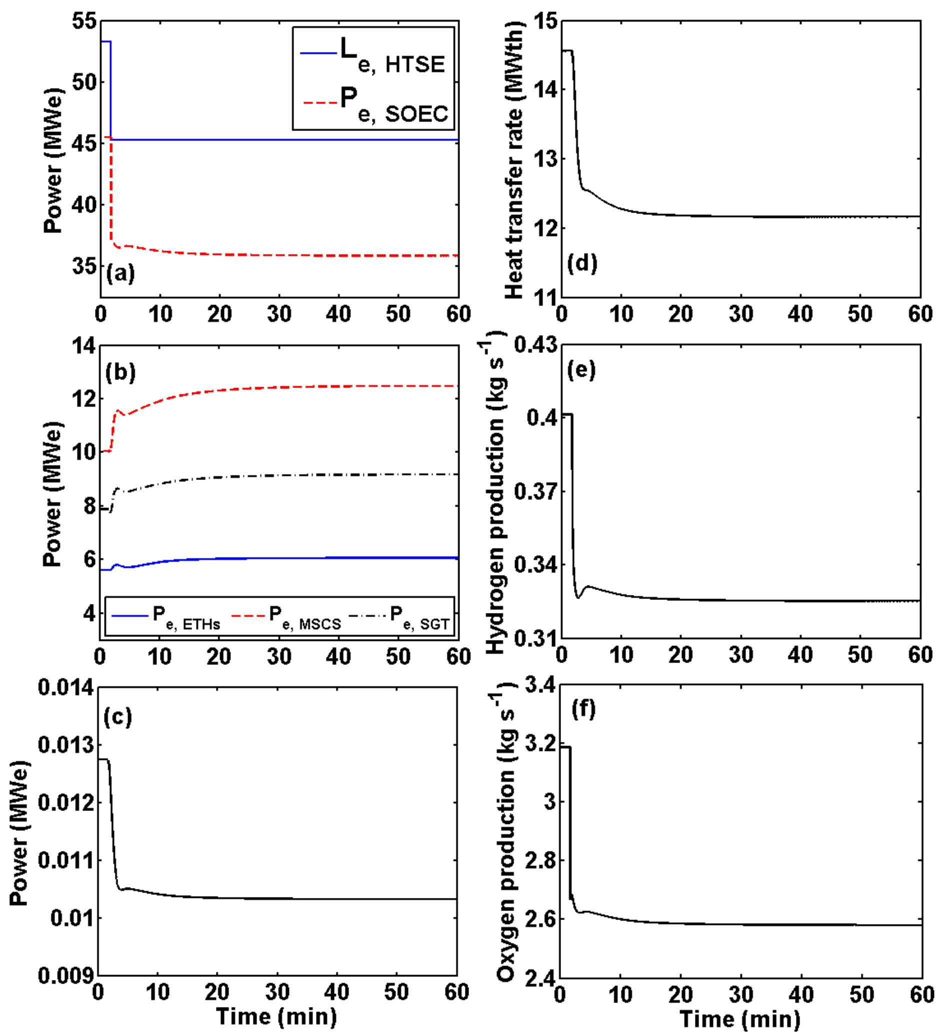

Figure 10. Case 1 results following a transient at 1.67 min: (a) VEL directed to the HTSE plant ($L_{e,\,HTSE}$) and electrical power consumption in the SOEC stacks ($P_{e,\,SOEC}$), (b) electrical power consumption in the ETHs ($P_{e,\,ETHs}$) and in the MSCS ($P_{e,\,MSCS}$), and electrical power production in the SGT ($P_{e,\,SGT}$), (c) electrical power consumption in the FWP, (d) rate of process heat flow across the HXs, (e) hydrogen production rate, and (f) oxygen production rate.

Figure 11 shows the responses of the CVs and MVs associated with the electrolyzer following the step change made in the electric load. The instantaneous fall in the SU factor visible in Figure 11(a) is attributed to the immediate drop in the reaction rate, resulting in less consumption of the steam during electrolysis. The FCV decreased its opening (Figure 11(c)) accordingly to decrease the cathode stream flow (Figure 11(b)), gradually increasing the SU factor back to its desired value within about 10 min. Note that this control strategy would result in a decreased utility consumption involved in heating the decreased cathode flow prior to entering the HTSE vessels. In Figure 11(d), a rapid drop in the cathode stream temperature at the SOEC stack outlet is observed immediately after the negative step change in the input load imposed. This is attributed to a decrease in the heat generated via irreversible losses, following the step decrease, which was not sufficient to provide the entire thermal energy consumed by the reaction. Consequently, the temperature decreased as the reaction proceeded along the cell. Subsequently, a decrease in the heat generated via irreversible losses was offset by the increased anode stream flow rate (Figure 11(e)), resulting in increased convective heating to the stack, thereby causing the stack temperature to rise back up to its set point. The outlet temperature was brought back to the set point by adjusting the opening of the corresponding FCV (Figure 11(f)) within about 45 min after the step change. Figure 12 shows the corresponding time series for the solid structure temperature gradient. As can be seen in the figure, the temperature gradient was kept lower than the maximum allowed temperature gradient (10°C cm^{-1} [20]), indicating that the stack was under safe operation during the simulation time. This result suggests that the proposed control strategy has a good potential to prevent the fracture of delicate stack components, which is related to the temperature fluctuations during dynamic operation of an SOEC stack.

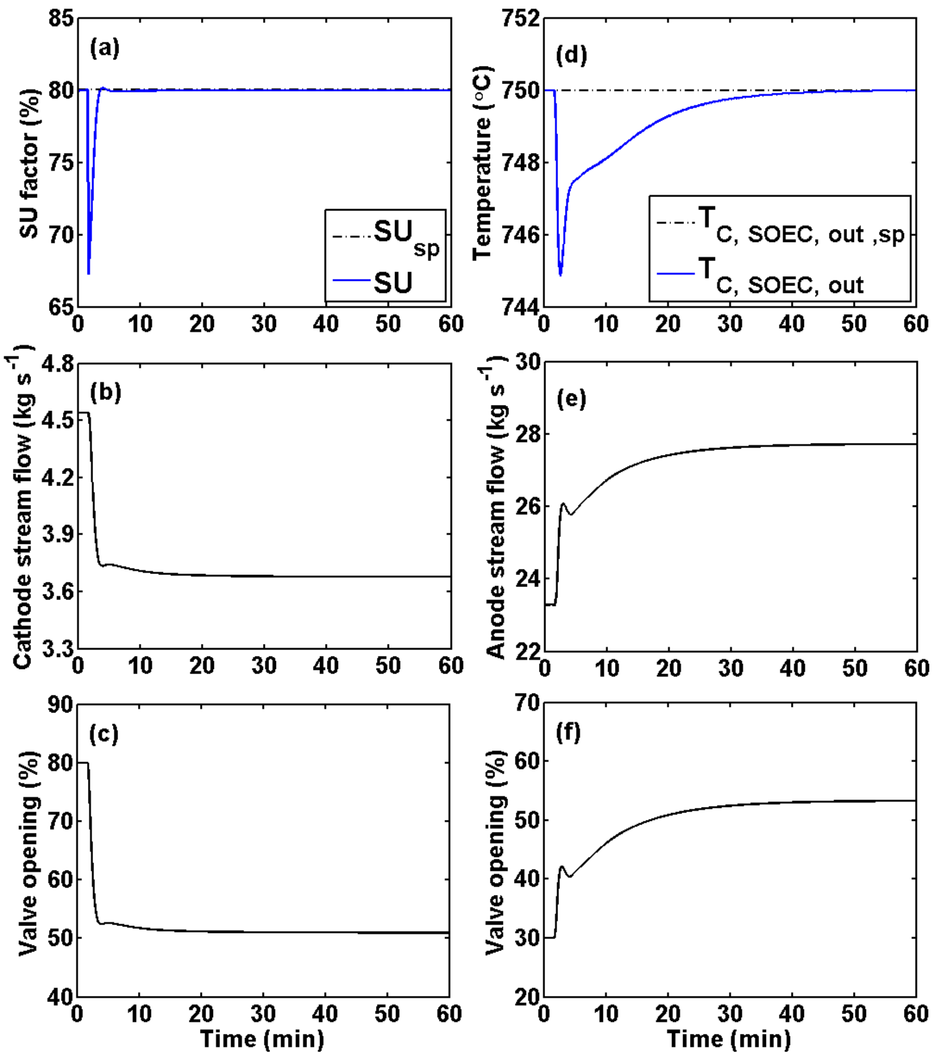

Figure 11. Case 1 results – *Electrolyzer*: (a) desired (SU_{sp}) vs. actual (SU) SU factor, (b) cathode stream flow entering the HTSE vessels, (c) valve opening of the FCV that regulates the cathode stream flow entering the HTSE vessels, (d) desired ($T_{C,\ SOEC,\ out,\ sp}$) vs. simulated cathode stream temperature at the SOEC stack outlet ($T_{C,\ SOEC,\ out}$), (e) anode stream flow entering the HTSE vessels, and (f) valve opening of the FCV that regulates the anode stream flow entering the HTSE vessels.

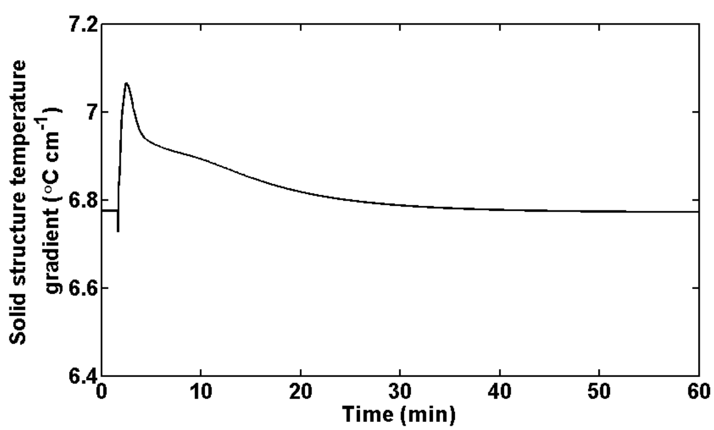

Figure 12. Case 1 result – *Electrolyzer*: solid structure temperature gradient.

Figure 13 shows the corresponding time series of the CVs and MVs in regard to the SOEC stack operating pressure, at both the cathode ($p_{C,\ SOEC}$) and anode ($p_{A,\ SOEC}$) sides. Initially, less consumption of the steam during electrolysis (due to the decreased electrical load input) resulted in more un-reacted steam flowing out of the stack (Figure 13(b)), thereby increasing $p_{C,\ SOEC}$ (Figure 13(a)). This also caused less oxygen flowing out of the stack (Figure 13(e)), resulting in an immediate fall in $p_{A,\ SOEC}$ (Figure 13(d)). As seen in Figures 13(c) and 13(f), the cathode and anode PCVs, respectively, adjusted their openings quickly to bring the pressures back to their set points. Note that the PCV openings are highly correlated to the corresponding stream flow rates so as to achieve the desired stack operating pressure.

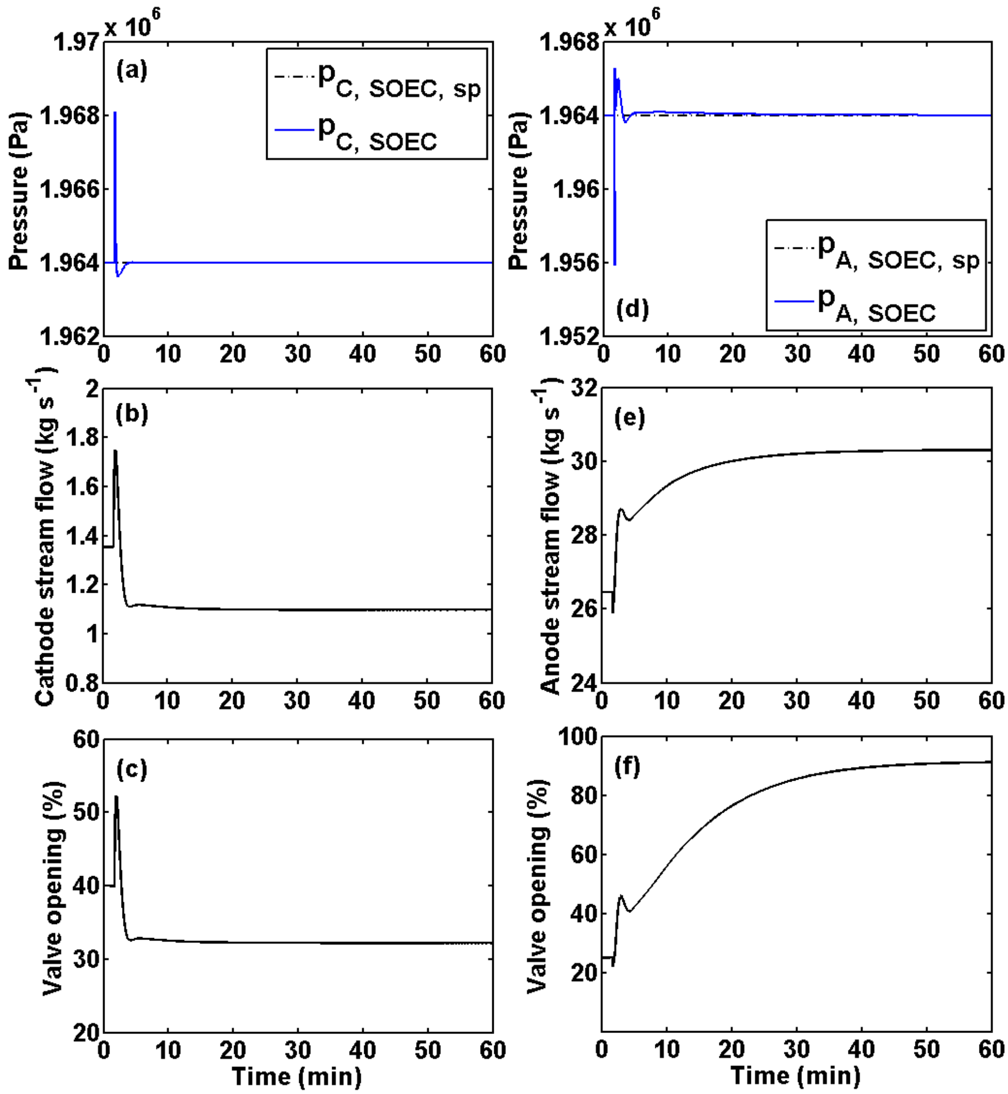

Figure 13. Case 1 results – *Electrolyzer*: (a) desired ($p_{C,\ SOEC,\ sp}$) vs. simulated ($p_{C,\ SOEC}$) SOEC stack operating pressure at the cathode side, (b) cathode stream flow exiting the HTSE vessels, (c) valve opening of the PCV that regulates the cathode stream flow exiting the HTSE vessels, (d) desired ($p_{A,\ SOEC,\ sp}$) vs. simulated ($p_{A,\ SOEC}$) SOEC stack operating pressure at the anode side, (e) anode stream flow exiting the HTSE vessels, and (f) valve opening of the PCV that regulates the anode stream flow exiting the HTSE vessels.

Figure 14 shows the electrical power produced from the SGT, which is essentially proportional to the flow rate of working fluid (see Figure 13(e)), provided that the fluid inlet temperature and pressure were maintained near their set-point values. The amount of the sweep gas compression work recovered by the SGT varied from 73.5% to 78.6% within the time window examined.

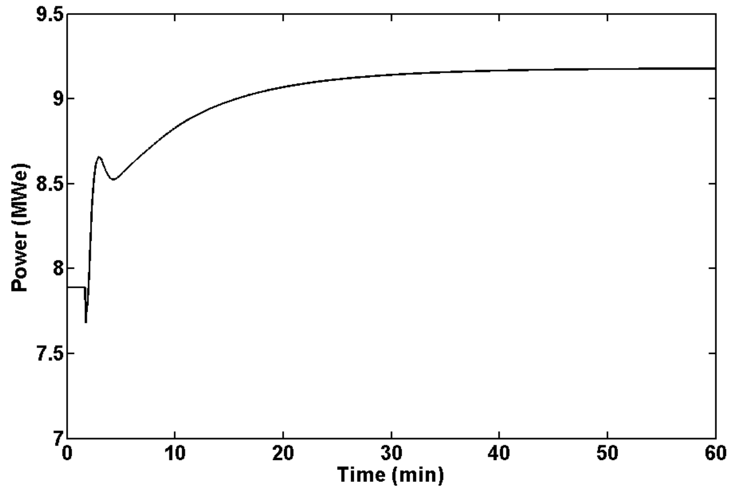

Figure 14. Case 1 result – *SGT*: electrical power production.

Figure 15 shows the simulation results regarding the FWP during a step change imposed on the $L_{e, HTSE}$. As for the same reason as in the case of $p_{C, SOEC}$, the cathode stream pressure at the FWP outlet immediately increased (Figure15(a)). While the cathode stream flow rate was reduced (Figure 15(d)), as a result of SU factor control, the MV was adjusted accordingly (Figure 15(b)) to maintain the CV at its set point, exhibiting about a five-minute settling time. As the pump speed and feedwater flow rate were reduced following the load step change, the power consumption in the FWP also decreased (Figure 15(c)).

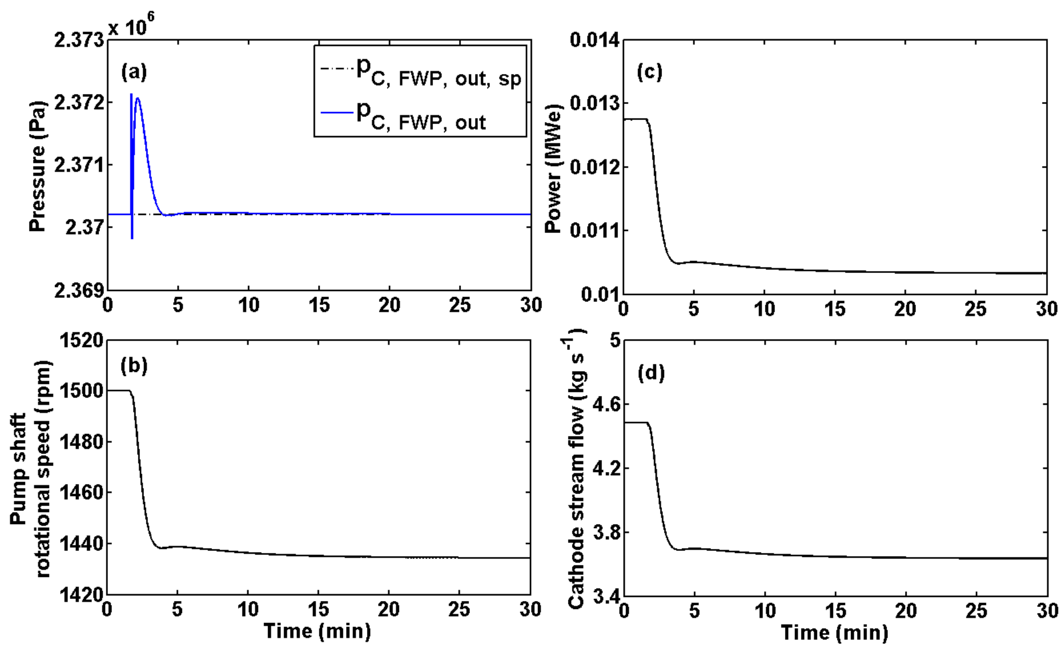

Figure 15. Case 1 results – *FWP*: (a) desired ($p_{C, FWP, out, sp}$) vs. simulated ($p_{C, FWP, out}$) cathode stream pressure at the FWP outlet, (b) pump shaft rotational speed, (c) power consumption, and (d) cathode stream (water) flow rate.

Figure 16 presents the simulation results for the MSCS with intercooling. For the same reason as discussed in the case of $p_{A,\ SOEC}$, the anode stream pressure at the MSCS outlet immediately decreased (Figure16(a)). While the anode stream flow rate was increased (Figure 16(d)), as a result of stack temperature control, the MV was adjusted accordingly (Figure 16(b)), bringing the CV back to its set point within about 20 min. As the compressor IGV angle and air flow rate were increased following the load step change, so did the power consumption in the MSCS (Figure 16(c)).

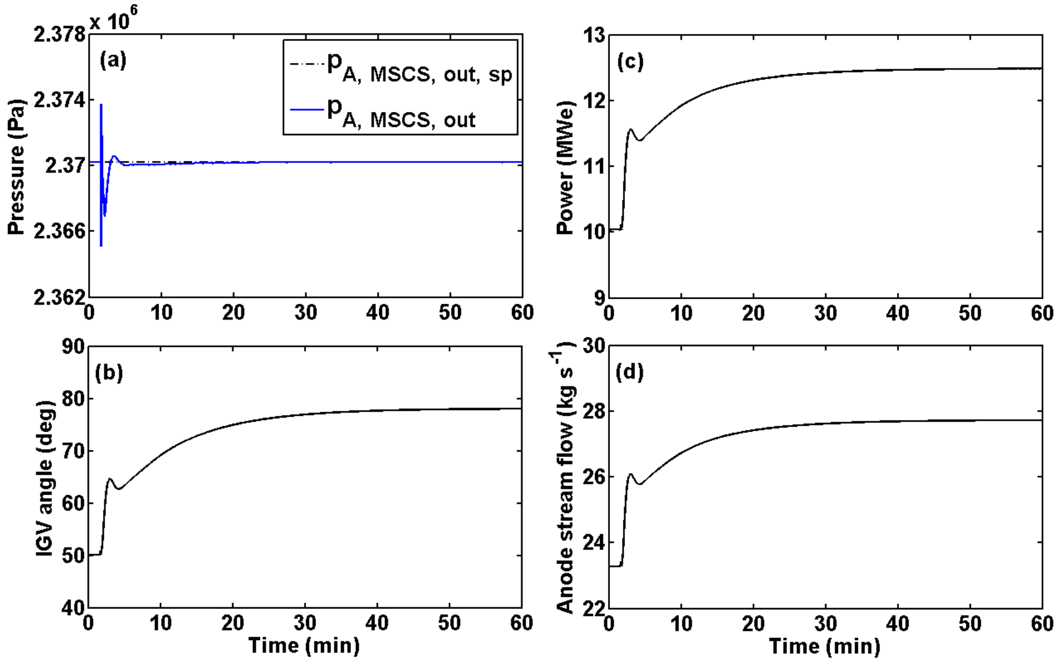

Figure 16. Case 1 results – *MSCS*: (a) desired ($p_{A,\ MSCS,\ out,\ sp}$) vs. simulated ($p_{A,\ MSCS,\ out}$) anode stream pressure at the MSCS outlet, (b) compressor IGV angle, (c) power consumption, and (d) anode stream (air) flow rate.

Figure 17 presents the transient responses associated with the nuclear-heat-recuperated HXs following the step change made in the $L_{e, HTSE}$. Initially, the outlet cathode stream temperature (Figure 17(a)) increased in response to the decreased cathode stream flow rate. The TCV decreased its opening (Figure 17(c)) accordingly in order to decrease the steam flowing through the cathode HX (Figure 17(b)). This facilitated decreased convective heat transfer between the steam drawn from the LWR and the cathode stream, and brought the temperature back to the set point within about 20 min after the step change. Conversely in Figure 17(d), the outlet anode stream temperature decreased in response to the increased anode stream flow rate. In this case, the TCV increased its opening (Figure 17(f)) in order to increase the steam flowing through the anode HX (Figure 17(e)), resulting in increased convective heat transfer between the steam drawn from the LWR and the anode stream. It required about 15 min for the anode stream temperature to match the corresponding set point and to settle to its final value.

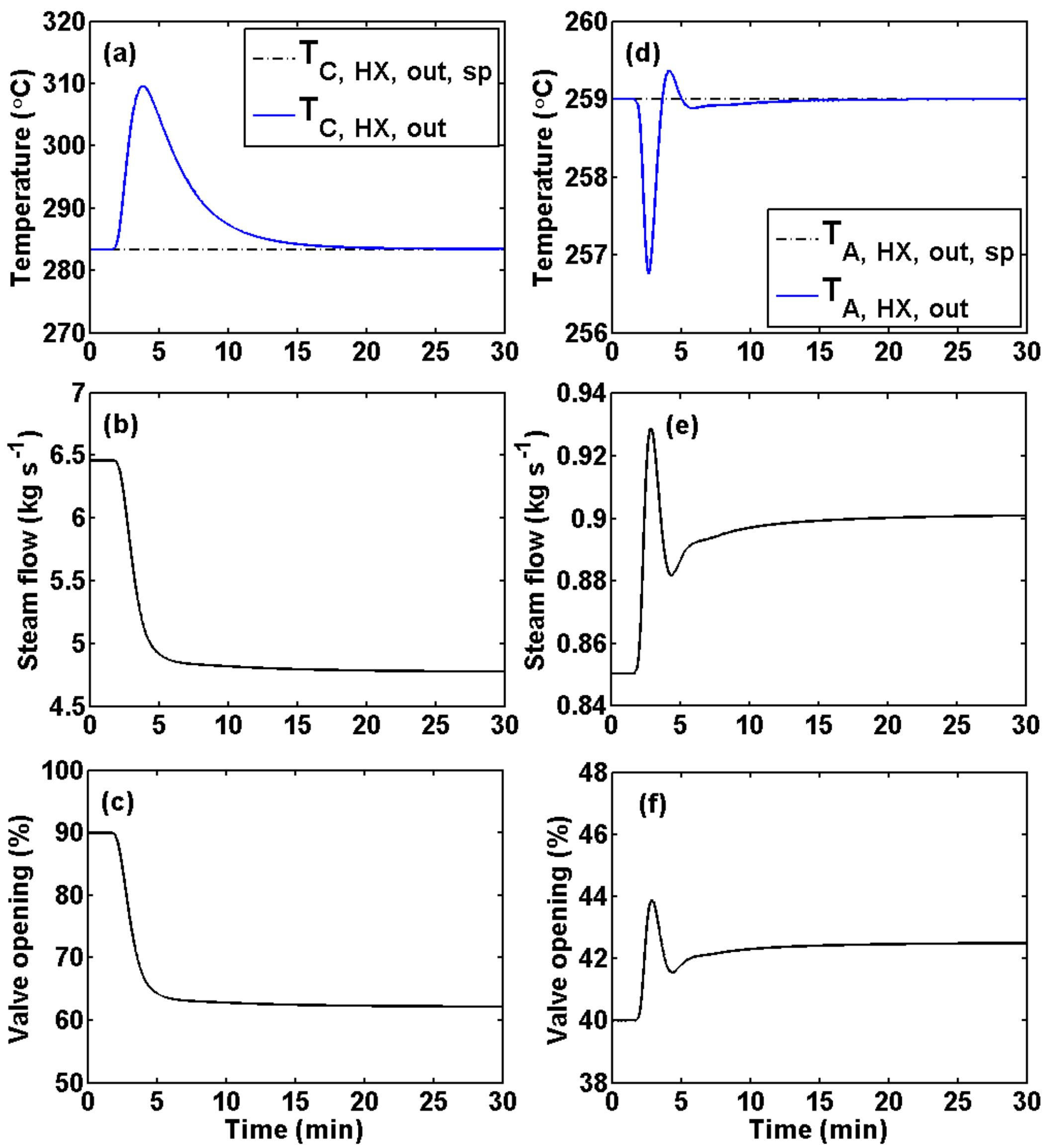

Figure 17. Case 1 results – *Nuclear-heat-recuperated HXs*: (a) desired ($T_{C, HX, out, sp}$) vs. simulated ($T_{C, HX, out}$) cathode stream temperature at the cathode HX outlet, (b) cathode stream flow rate, (c) valve opening of the TCV that regulates the steam flow entering the cathode HX, (d) desired ($T_{A, HX, out, sp}$) vs. simulated ($T_{A, HX, out}$) anode stream temperature at the anode HX outlet, (e) anode stream flow rate, and (f) valve opening of the TCV that regulates the steam flow entering the anode HX.

Figure 18 presents the transient responses associated with the ETHs. They show essentially the same results as in Figure 17 but with a different MV, i.e. an electric current. The fall (Figure 18(c)) and rise (Figure 18(f)) in the electric current caused the cathode and anode stream temperatures to decrease (Figure 18(a)) and increase (Figure 18(d)) by consuming less (Figure 18(b)) and more (Figure 18(e)) electricity in the ETHs, respectively. The observed settling times of the CVs are 10 min and 20 min for the cathode and anode stream temperatures, respectively.

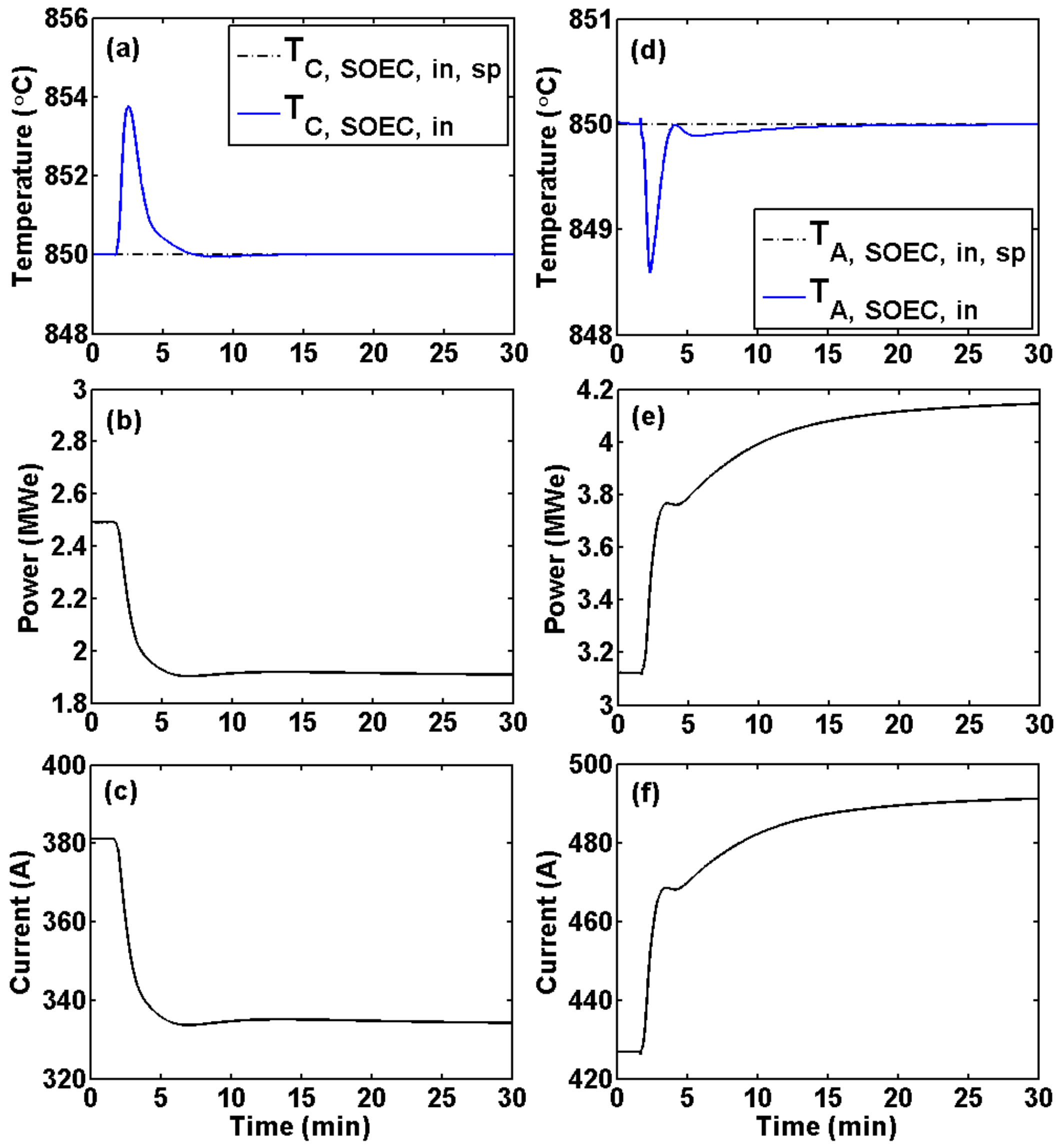

Figure 18. Case 1 results – *ETHs*: (a) desired ($T_{C,\ SOEC,\ in,\ sp}$) vs. simulated ($T_{C,\ SOEC,\ in}$) cathode stream temperature at the SOEC stack inlet, (b) electric load for an ETH that heats up the cathode stream, (c) electric current for the cathode stream ETH, (d) desired ($T_{A,\ SOEC,\ in,\ sp}$) vs. simulated ($T_{A,\ SOEC,\ in}$) anode stream temperature at the SOEC stack inlet, (e) electric load for an ETH that heats up the anode stream, and (f) electric current for the anode stream ETH.

Figure 19 shows the corresponding time series regarding the H_2/steam mixer. The rise in the cathode stream H_2 mole fraction (Figure 19(a)) is attributed to the fall in the inlet cathode stream (pure steam) flow, due to SU factor control, prior to entering the mixer (Figure 19(b)). The H_2 mole fraction in the mixture settled to its set point, with a small interim excursion (an increase of 0.8%) within 6 min, by progressively reducing the amount of hydrogen recycled from the product stream (Figure 19(c)).

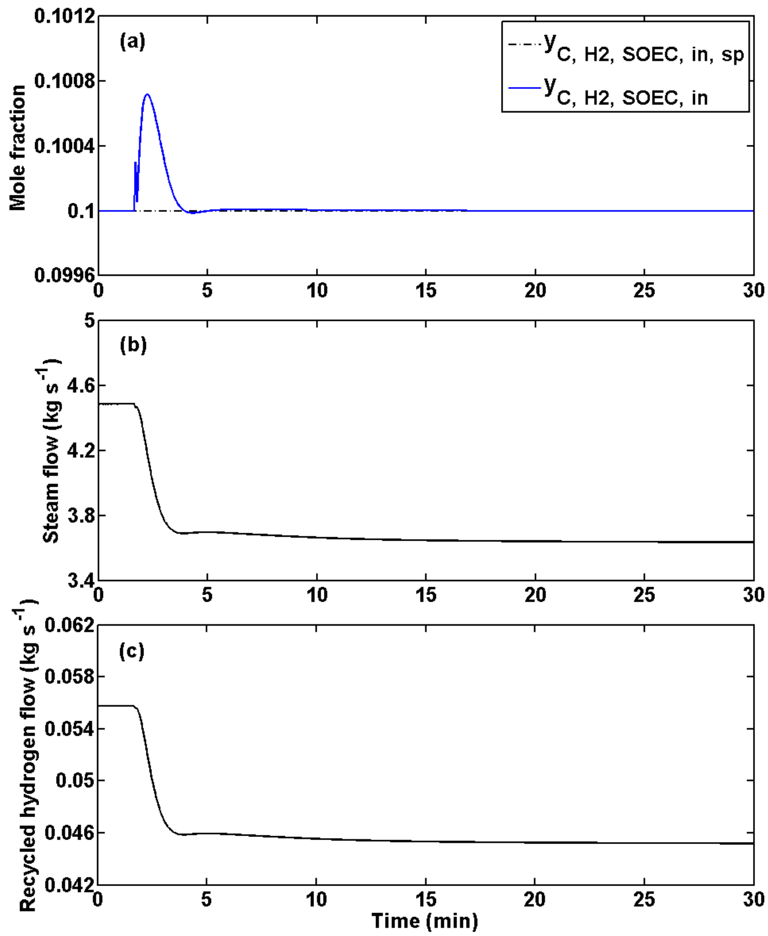

Figure 19. Case 1 results – *H_2/steam mixer*: (a) desired ($y_{C, H2, SOEC, in, sp}$) vs. simulated ($y_{C, H2, SOEC, in}$) cathode stream H_2 mole fraction at the SOEC stack inlet, (b) steam flow rate, and (c) recycled hydrogen flow rate.

Figure 20(b)–(h) compares the output responses for a disturbance (i.e., VEL) change with the FY16 (blue solid line) and FY17 (red dashed line) HTSE plant models. The initial and final load levels (Figure 20(a)) were chosen such that the corresponding hydrogen production rates obtained from both models were same. It is clear from the figures that the controller settings implemented in the FY17 model provided superior output responses, with much smaller settling times than those resulting from the FY16 model. In addition, by comparison, the output responses from the FY17 model had smaller maximum deviations and were less oscillatory.

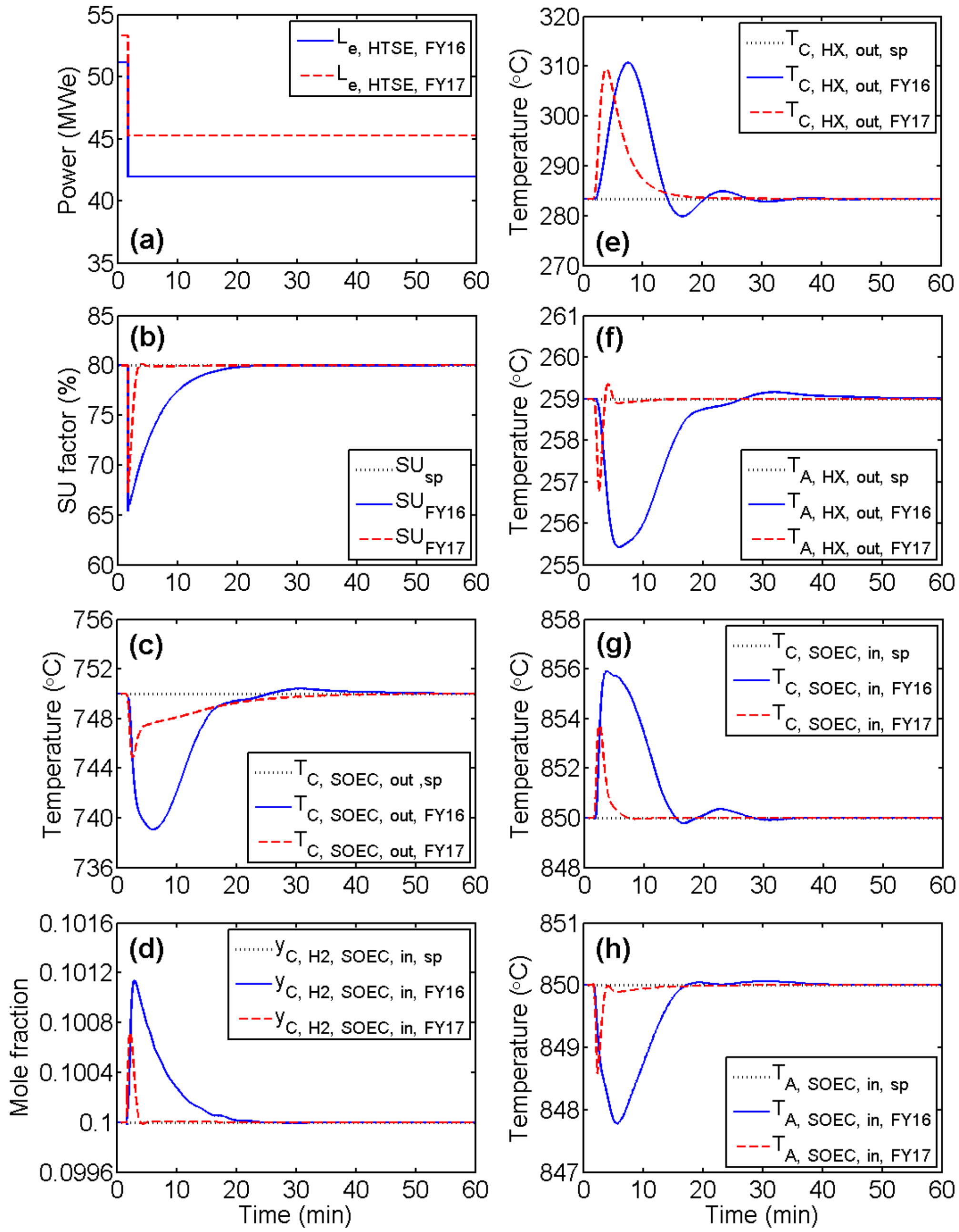

Figure 20. Model comparisons (FY16 vs. FY17): (a) VEL directed to the HTSE plant ($L_{e, HTSE}$), (b) SU factor (*SU*), (c) cathode stream temperature at the SOEC stack outlet ($T_{C, SOEC, out}$), (d) cathode stream H_2 mole fraction at the SOEC stack inlet ($y_{C, H2, SOEC, in}$), (e) cathode stream temperature at the cathode HX outlet ($T_{C, HX, out}$), (f) anode stream temperature at the anode HX outlet ($T_{A, HX, out}$), (g) cathode stream temperature at the SOEC stack inlet ($T_{C, SOEC, in}$), and (h) anode stream temperature at the SOEC stack inlet ($T_{A, SOEC, in}$).

4.2 Case 2: Load-following Responses with PV Solar Power

In Case 2, the load-following capability of the proposed HTSE plant (as a flexible load resource) under variable PV solar power generation was demonstrated. Figures 21 and 22 show the time series of a VEL (i.e., PV solar power plus a constant minimum load [24 MW_e]) delivered to the plant, hydrogen and oxygen production rates, and selected CVs simulated for one week. As can be seen in the figures, the plant can maintain all the CVs (red solid lines in Figure 22) near their desired set points (black dotted lines in Figure 22) regardless of the time-varying electrical load delivered to the plant (Figure 21(a)), while supporting hydrogen and oxygen production (Figure 21 (b)). These results suggest that the HTSE process integrated N-R HES, with a high penetration of renewable generation, has a good potential to act as a highly responsive device to meet load-following needs by accordingly delivering the necessary electricity generation profile demanded by the electric grid, while correspondingly adjusting itself to maintain adequate operating conditions. Moreover, since the HTSE plant can be operated at its minimum turndown for as long as requested, the N-R HES configuration including the HTSE plant can maintain the change in its electrical production for a sufficient duration.

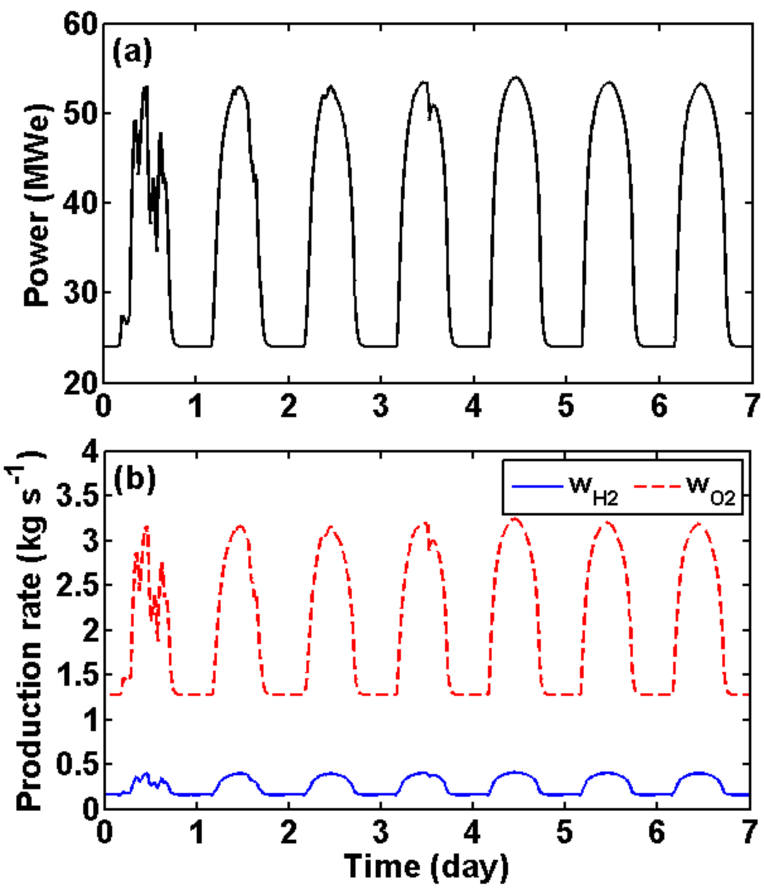

Figure 21. Case 2 results: (a) PV solar power generation, and (b) hydrogen (w_{H2}) and oxygen (w_{O2}) production rates.

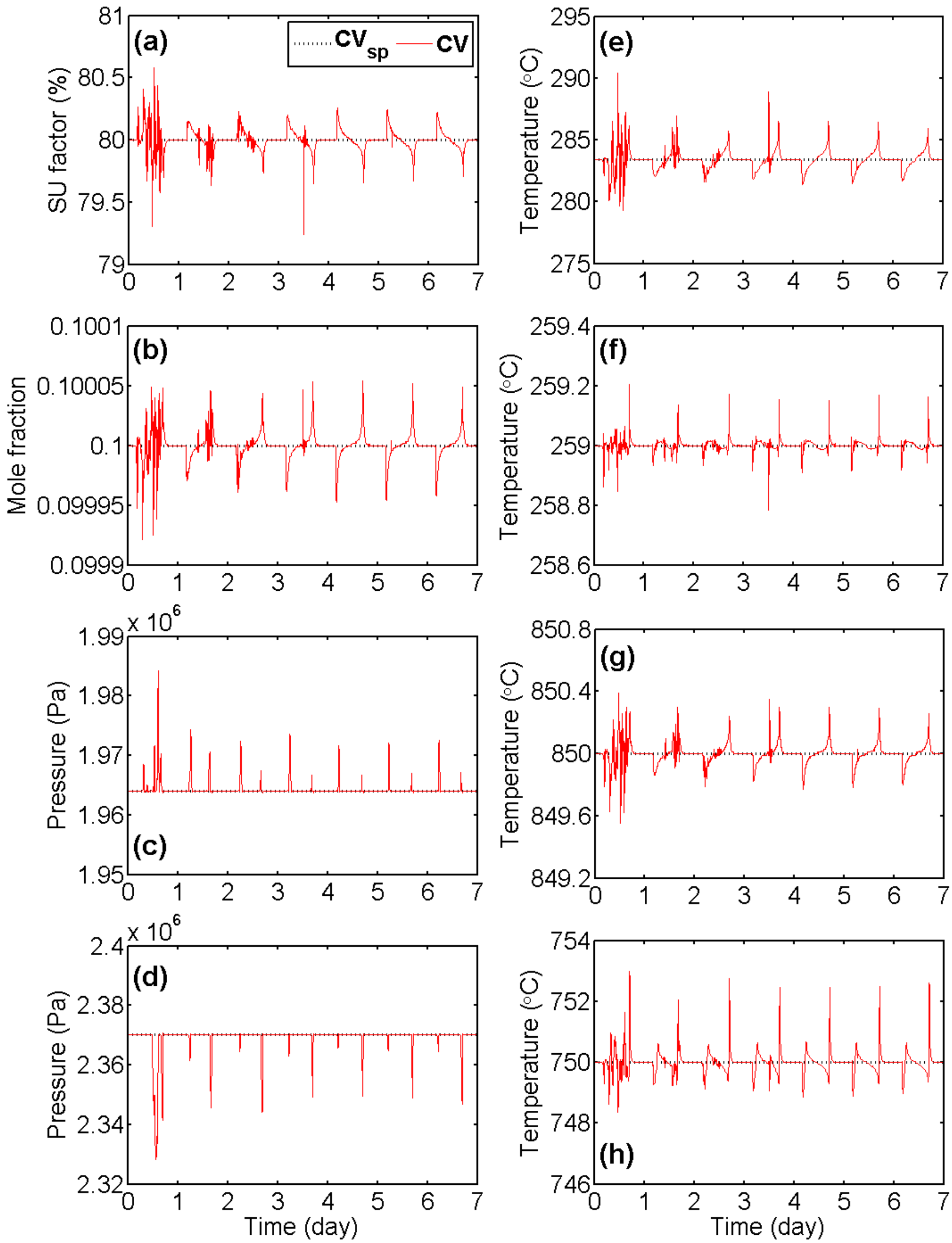

Figure 22. Case 2 results: (a) SU factor, (b) cathode stream H_2 mole fraction at the SOEC stack inlet, (c) SOEC stack operating pressure at the anode side, (d) cathode stream pressure at the FWP outlet, (e) cathode stream temperature at the cathode HX outlet, (f) anode stream temperature at the anode HX outlet, (g) cathode stream temperature at the SOEC stack inlet, and (h) cathode stream temperature at the SOEC stack outlet.

4.3 Case 3: Load-following Responses with Wind Power

This test was designed to assess the capability of the same system considered in Case 2 for load following, but in coordination with wind power generation. The results simulated for one week are plotted in Figures 23 and 24. Similar to the results shown in Case 2, the variability introduced by the renewable (wind) source was essentially accommodated by the use of the flexible electrical load provided by the HTSE plant. The plant could maintain all the CVs close to their set-point values at all times, exhibiting satisfactory control performance over the entire range of HTSE operating conditions.

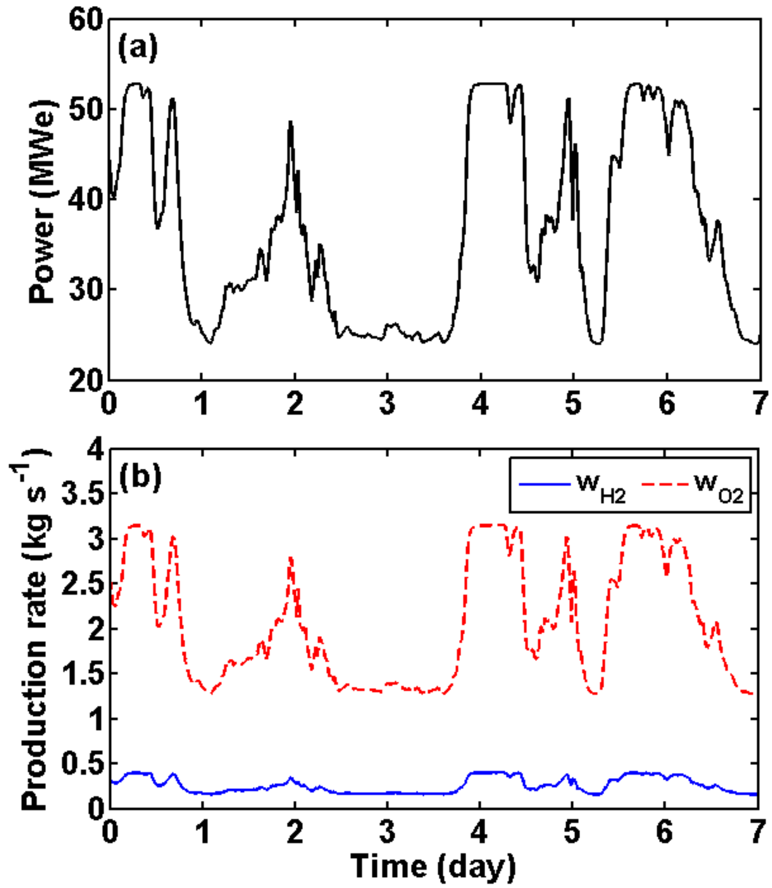

Figure 23. Case 3 results: (a) wind power generation, and (b) hydrogen (w_{H2}) and oxygen (w_{O2}) production rates.

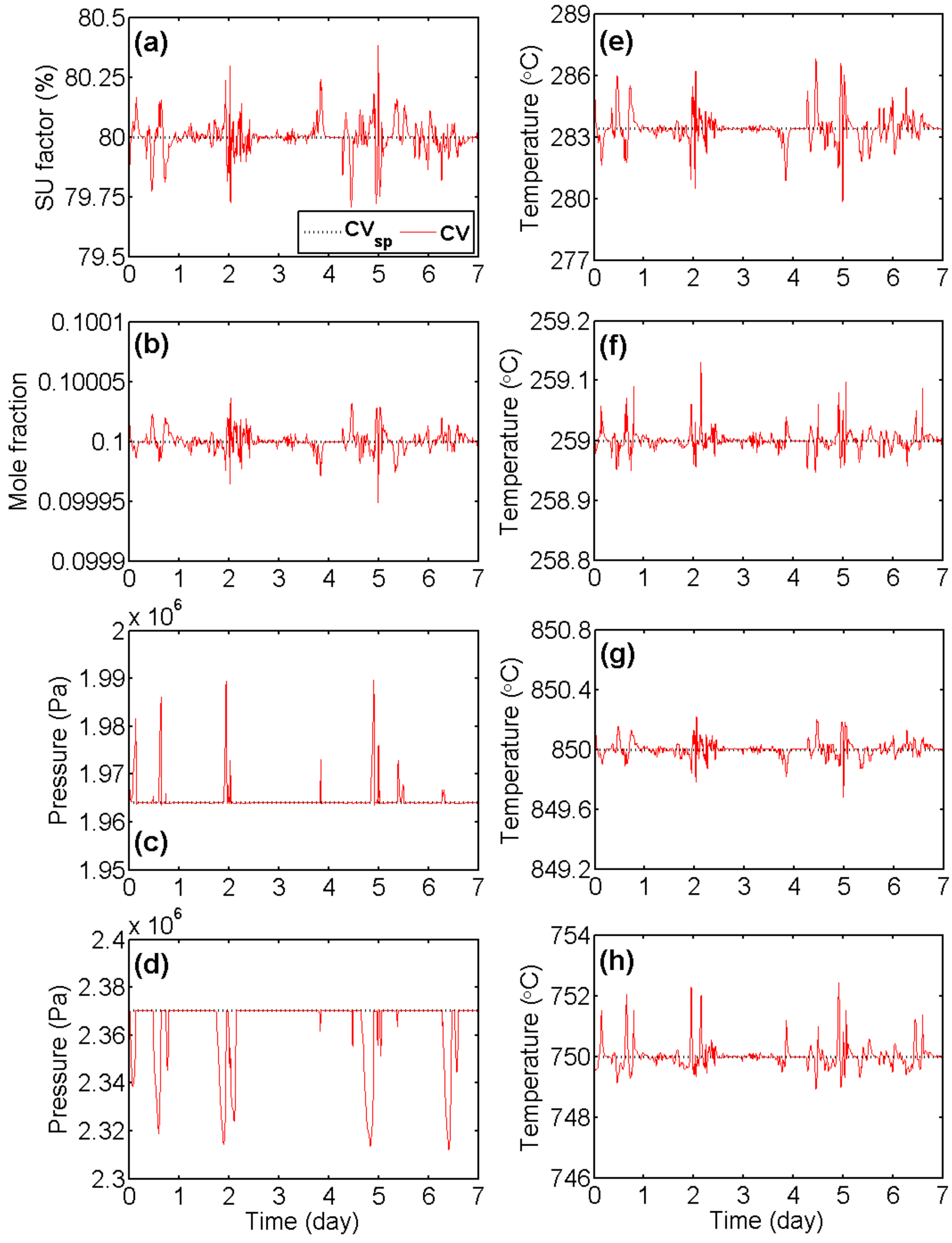

Figure 24. Case 3 results: (a) SU factor, (b) cathode stream H_2 mole fraction at the SOEC stack inlet, (c) SOEC stack operating pressure at the anode side, (d) cathode stream pressure at the FWP outlet, (e) cathode stream temperature at the cathode HX outlet, (f) anode stream temperature at the anode HX outlet, (g) cathode stream temperature at the SOEC stack inlet, and (h) cathode stream temperature at the SOEC stack outlet.

5. CONCLUSIONS

The M&S framework to assess the economic viability of an N-R HES is reaching the maturity level necessary to begin analysis of realistic cases. In particular, the FY16 Modelica model developed for an integration of the HTSE process with an LWR has been modified and improved to include several new key components of the system, such as an FWP, an MSCS, an SGT, FCVs, and PCVs. In addition, the control parameters have been tuned based on process models.

A dynamic performance analysis of the improved LWR/HTSE integration case was carried out to evaluate the technical feasibility and safety of such a system operating under highly variable conditions requiring flexible output. The case study results clearly indicate that the FY17 model results in output responses far superior to those observed with the FY16 model. Simulation results show that the suggested control scheme can maintain the CVs within desired limits under various plant operating conditions. The analysis also shows that the proposed HTSE plant, when integrated within an N-R HES, can respond quickly and maintain the required change for a sufficient duration in response to large, rapid net demand variations. The ability for HTSE to respond quickly can support renewable integration and various types of ancillary services, such as operating reserves (regulating, ramping, and load following). Its operational flexibility and the variety of potential N-R HES configurations in which it can be integrated make HTSE a good candidate for integration from a technical point of view.

REFERENCES

[1] Bragg-Sitton S, Boardman R. Overview of U.S. DOE Research and Development of Nuclear-Renewable Hybrid Energy Systems. Transactions of the American Nuclear Society. 2015;112:113-6.

[2] Bragg-Sitton SM, Boardman R, Rabiti C, Kim JS, McKellar M, Sabharwall P, et al. Nuclear-Renewable Hybrid Energy Systems: 2016 Technology Development Program Plan. Idaho Falls (ID): Idaho National Laboratory, Nuclear Science and Technology Division; 2016 Mar. Report No.:INL/EXT-16-38165. Contract No.:DE-AC07-05ID14517. Sponsored by the U.S. Department of Energy.

[3] Chen J, Garcia HE, Kim JS, Bragg-Sitton SM. Operations optimization of nuclear hybrid energy systems. Nuclear Technology. 2016;195:143-56.

[4] Garcia HE, Chen J, Kim JS, McKellar MG, Deason WR, Vilim RB, et al. Nuclear Hybrid Energy Systems - Regional Studies: West Texas & Northeastern Arizona. Idaho Falls (ID): Idaho National Laboratory, Nuclear Science and Technology Division; 2015 Apr. Report No.:INL/EXT-15-34503. Contract No.:DE-AC07-05ID14517. Sponsored by the U.S. Department of Energy.

[5] Garcia HE, Chen J, Kim JS, Vilim RB, Binder WR, Bragg Sitton SM, et al. Dynamic performance analysis of two regional Nuclear Hybrid Energy Systems. Energy. 2016;107:234-58.

[6] Kim J, Garcia H. Nuclear-Renewable Hybrid Energy System for Reverse Osmosis Desalination Process. Transactions of the American Nuclear Society. 2015;112:121-4.

[7] Fritzson P. Principles of Object-Oriented Modeling and Simulation with Modelica 3.3: A Cyber-Physical Approach: John Wiley & Sons; 2014.

[8] Kim JS, McKellar M, Bragg-Sitton SM, Boardman RD. Status on the Component Models Developed in the Modelica Framework: High-Temperature Steam Electrolysis Plant & Gas Turbine Power Plant. Idaho Falls (ID): Idaho National Laboratory, Nuclear Science and Technology Division; 2016 Oct. Report No.:INL/EXT-16-40305. Contract No.:DE-AC07-05ID14517. Sponsored by the U.S. Department of Energy.

[9] Dassault Systems. DYMOLA Systems Engineering [Internet]. [updated 2017 Aug 2; cited 2017 Aug 11]. Available: https://www.3ds.com/products-services/catia/products/dymola/.

[10] Modelica Association. Modelica Standard Library [Internet]. [updated 2016 Apr 3; cited 2017 Aug 11]. Available: https://github.com/modelica/Modelica.

[11] Casella F, Leva A. ThermoPower [Internet]. [updated 2014 Jun 10; cited 2017 Aug 11]. Available: https://github.com/modelica-3rdparty/ThermoPower.

[12] Modelica Association. Modelica Conventions [Internet]. [updated 2013 Sep 23; cited 2017 Aug 11]. Available: http://simulationresearch.lbl.gov/modelica/releases/msl/Modelica%203.2.1/help/Modelica_UsersGuide_Conventions.html#Modelica.UsersGuide.Conventions.

[13] Epiney AS, Kinoshita RA, Kim JS, Rabiti C, Greenwood MS. Software development infrastructure for the HYBRID modeling and simulation project. Idaho Falls (ID): Idaho National Laboratory,

Nuclear Science and Technology Division; 2016 Sep. Report No.:INL/EXT-16-40004. Contract No.:DE-AC07-05ID14517. Sponsored by the U.S. Department of Energy.

[14] Sun X, Chen M, Jensen SH, Ebbesen SD, Graves C, Mogensen M. Thermodynamic analysis of synthetic hydrocarbon fuel production in pressurized solid oxide electrolysis cells. International Journal of Hydrogen Energy. 2012;37:17101-10.

[15] Kim JS, Powell KM, Edgar TF. Nonlinear model predictive control for a heavy-duty gas turbine power plant. 2013 American Control Conference2013. p. 2952-7.

[16] O'Brien JE, McKellar MG, Harvego EA, Stoots CM. High-temperature electrolysis for large-scale hydrogen and syngas production from nuclear energy – summary of system simulation and economic analyses. International Journal of Hydrogen Energy. 2010;35:4808-19.

[17] Seborg DE, Mellichamp DA, Edgar TF, Doyle III FJ. Process dynamics and control: John Wiley & Sons; 2010.

[18] Kim JS, Chen J, Garcia HE. Modeling, control, and dynamic performance analysis of a reverse osmosis desalination plant integrated within hybrid energy systems. Energy. 2016;112:52-66.

[19] O'Brien J. Thermodynamic considerations for thermal water splitting processes and high temperature electrolysis. ASME 2008 International Mechanical Engineering Congress and Exposition. Boston, Massachusetts, USA: American Society of Mechanical Engineers; 2008. p. 639-51.

[20] Aguiar P, Adjiman CS, Brandon NP. Anode-supported intermediate temperature direct internal reforming solid oxide fuel cell. I: model-based steady-state performance. Journal of Power Sources. 2004;138:120-36.

APPENDIX

Table A. PI controller settings based on the DS method.

CTRL No. (model order - F: 1st S: 2nd)	Model gain K	Sum of time constants [dominant time constant] τ (s)	Desired closed-loop time constant τ_c^b(s)	Time delay θ (s)	CTRL gain K_c	Integral time τ_I (s)	Lower bound on CTRL output y^{min}	Upper bound on CTRL output y^{max}
1 (F)	252 (K^c)	160	107	0	5.94×10^{-3} (K^{-1})	160	0.05	1
2 (F)	120 (K)	76.0	50.6	0	0.0125 (K^{-1})	76.0	0.05	1
3 (F)	1 (unitless)	8	2.67	0	3 (unitless)	8	2.79×10^{-3} (kg s^{-1})	0.0669 (kg s^{-1})
4 (S)	1.20 (K A^{-1})	18.7 [13.1]	6.53	0	2.38 (A K^{-1})	18.7	0	457 (A^d)
5 (S)	0.561 (K A^{-1})	19.9 [12.9]	4.30	0	8.23 (A K^{-1})	17.2	0	640 (A)
6 (S)	48.7 (K)	216 [213]	213	0	0.0199 (K^{-1})	213	0.05	1
7 (F)	0.303 (kg s^{-1})	1.17	2.34	0	4.23×10^{-3} (s kg^{-1})	1.17	0.05	1
8 (F)	699 (Pa rpm^{-1})	7.86	2.62	0	4.29×10^{-3} (rpm Pa^{-1})	7.86	1125 (rpm)	1875 (rpm)
9[a]	N/A	N/A	N/A	N/A	N/A	0.304	46.7 (deg)	85 (deg)
10 (F)	-2.77×10^{5} (Pa)	2.54	0.507	0	-1.81×10^{-5} (Pa^{-1})	2.03	0.05	1
11 (F)	-4.74×10^{5} (Pa)	4.3	0.860	0	-1.05×10^{-5} (Pa^{-1})	3.44	0.05	1

[a] Controller settings for CTRL 9 were adapted from Ref. [8].

[b] Setting $\tau_c = \tau_I/x$ means that the desired closed-loop response is x times faster than the open-loop response.

[c] Kelvin

[d] Ampere